Berger, W.H., Kroenke, L.W., Mayer, L.A., et al., 1993
Proceedings of the Ocean Drilling Program, Scientific Results, Vol. 130

21. QUATERNARY OXYGEN ISOTOPE RECORD OF PELAGIC FORAMINIFERS: SITE 805, ONTONG JAVA PLATEAU[1]

W.H. Berger,[2] T. Bickert,[3] H. Schmidt,[3] G. Wefer,[3] and M. Yasuda[2]

ABSTRACT

The oxygen isotope records of *G. sacculifer* and *Pulleniatina* in the uppermost three cores at Ocean Drilling Program Hole 805C span the last 1.6 m.y., an estimate based on Fourier stratigraphy. The last 700,000 yr are dominated by both eccentricity- and obliquity-related orbital fluctuations. The range of variation of $\delta^{18}O$ values is about 1.5‰, of which ca. 75% may be assigned to global ice-volume effect. The remainder of the range is shared by the effects of surface temperature variation, thermocline depth change (in the case of *Pulleniatina,* especially), and differential dissolution.

Before 1 Ma, obliquity-related fluctuations dominate. The transition between obliquity- and eccentricity-dominated time occurs between ca. 1 and 0.7 Ma. It is marked by irregularities in phase relationships, the source of which is not clear. The age of the Brunhes/Matuyama boundary is determined as 794,000 yr by obliquity counting. However, an age of 830,000 yr also is compatible with the counts of both eccentricity and obliquity cycles. In the first case, Stage 19 (which contains the boundary) is coincident with the crest of the 19th obliquity cycle, setting the first crest downcore equal to zero, and counting backward (o19). In the second, Stage 19 coincides with o20.

No evidence was found for fluctuations related to precession (23 and 19 k.y.) rising above the noise level, using plain Fourier expansion on the age model of the entire series.

Detailed stratigraphic comparison with the Quaternary record of Hole 806B allows the recognition of major dissolution events (which increase the difference in $\delta^{18}O$ values of *G. sacculifer* at the two sites). These occur at Stages 11–13, 16–17, and near 1.5 Ma (below o33).

INTRODUCTION

The Ontong Java Plateau straddles the equator and bears a thick cover of calcareous sediments. Already these sediments have contributed much information on the stable isotope stratigraphy of the Quaternary (Shackleton and Opdyke, 1973, 1976; Schiffelbein, 1984; Hebbeln et al., 1990; Wu and Berger, 1991), as well as to that of the Neogene in general (Woodruff et al., 1981; Whitman and Berger, 1992). Extensive work on box cores (Johnson et al., 1977; Berger et al., 1978, 1987) provides detailed background information on present-day conditions of sedimentation, back to the last glacial.

During Leg 130 of the Ocean Drilling Program (ODP), advanced hydraulic piston coring (APC) was used to retrieve a number of undisturbed sequences within the Neogene (Fig. 1). We have reported on the stable isotope stratigraphy of the uppermost five cores of Hole 806B elsewhere in this volume (Berger et al., this volume; Bickert et al., this volume; Schmidt et al., this volume). For comparison with this record, we selected the first three cores from Hole 805C (1°13.69′N, 160°31.77′E; water depth, 3188 m) for detailed study of the Quaternary. These cores (130-805C-1H through -3H) comprise the upper 26.8 m of sediment, which consists of calcareous ooze with foraminifers and nannofossils. Preservation is quite good on the whole. The period represented by the sequence sampled is about 1.6 m.y. long.

Our goal is to provide, together with the companion study on Hole 806B (Berger et al., this volume), a more detailed and reliable Quaternary oxygen isotope stratigraphy for the western equatorial Pacific than has been available. The record of Site 805 should add information on the effects of dissolution on the $\delta^{18}O$ stratigraphy. The site is situated just above the regional lysocline (at about 3300 m; Berger et al., 1982), but close enough to experience the effects of dissolution, especially whenever the lysocline rises to a shallow level (Hebbeln et al., 1990; Groetsch et al., 1991; Le and Shackleton, 1992). The sedimentation rate (about 17 m/m.y.) is adequate for the resolution here attempted.

MATERIALS AND METHODS

Cores Studied

The three uppermost cores at Hole 805C were taken from 0 to 7.8, 7.8 to 17.3, and 17.3 to 26.8 mbsf. Their lengths are 7.80, 9.88, and 9.40 m (recovery: 100%, 104%, and 99%, respectively). The cores contain light gray to white (downward in the section) foraminifer nannofossil ooze and nannofossil ooze with foraminifers. The sediment is moderately bioturbated. Mottled color banding is common and appears to be cyclic in places. Minor drilling disturbances are seen at the very top of Cores 130-805C-2H and -3H.

Sample Preparation

Cores 130-805C-1H through -3H were sampled at 10-cm intervals, from near the surface to 26.8 mbsf. Approximately 5 g of wet bulk sediment were freeze-dried for each sample, weighed, and wet-sieved at 63 µm. The material was exposed to ultrasound twice for about 10 s during the process. The sand fraction (>63 µm) was dried in an oven at 50°C for 40 hr, and then weighed again to determine the percent sand fraction.

For each sample, 25 tests of the planktonic foraminifer taxa *Globigerinoides sacculifer* and *Pulleniatina* were picked in the 355–425 µm fraction and crushed with a glass pestle. In some cases, fewer than 25 tests were available. The number of specimens (25) and the rather narrow size fraction were chosen to minimize the influence of vital effects on the isotopic ratios (Berger et al., 1978). For *G. sacculifer,* only tests that were intact were selected. An effort was made to avoid *G. fistulosus* where present; the immature members of the species are difficult to distinguish from mature *G. "trilobus"* (the

[1] Berger, W.H., Kroenke, L.W., Mayer, L.A., et al., 1993. *Proc. ODP, Sci. Results,* 130: College Station, TX (Ocean Drilling Program).

[2] Geological Research Division, Scripps Institution of Oceanography, University of California, San Diego, La Jolla, CA 92093, U.S.A.

[3] Fachbereich Geowissenschaften, Universität Bremen, Postfach 330440, D-2800 Bremen 33, Federal Republic of Germany.

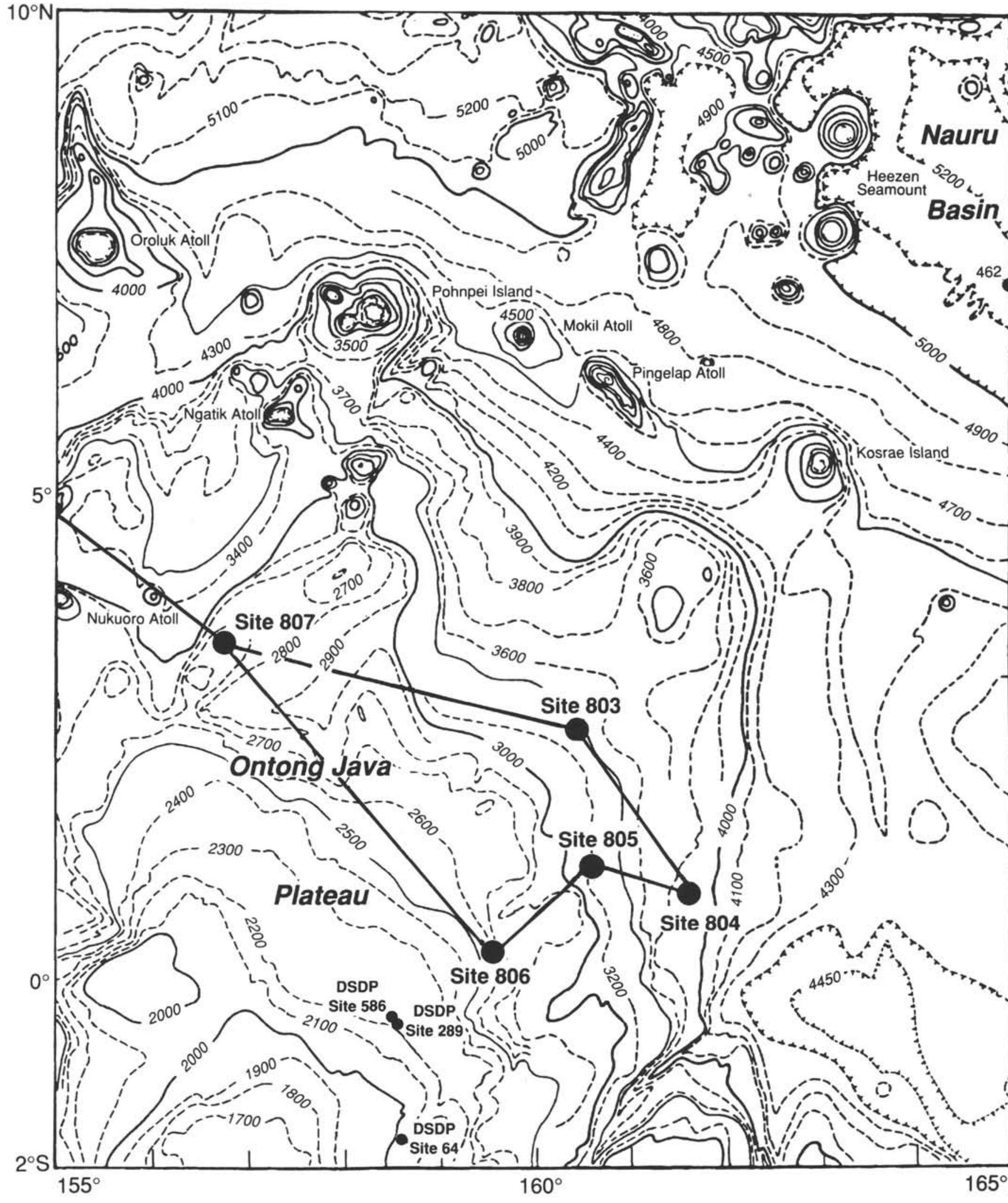

Figure 1. Track of Leg 130 on Ontong Java Plateau and position of sites (from Berger et al., 1991).

non-"sac" phenotype of *G. sacculifer*). The sample size for isotopic measurements was 60–80 μg; the carbonate was reacted with phosphoric acid at 75°C. Isotopic ratios were determined using a Finnigan MAT 251 Micromass spectrometer with a Finnigan Automated Carbonate Device, at the Geoscience Department of the University of Bremen. Precision was regularly checked by running standards (Solnhofen Limestone). Over a 1-yr period (1990), standard deviations were <0.07‰ for $\delta^{18}O$ and 0.5‰ for $\delta^{13}C$. Conversion to the PeeDee Belemnite (PDB) scale was performed by means of the NBS-18, NBS-19, and NBS-20 standards.

Interpretation of Oxygen Isotopes

The methodology of interpreting the oxygen isotopes in pelagic foraminifers is summarized in Berger and Gardner (1975) and Wefer and Berger (1991). The basis for interpretation is the well-known paleotemperature equation of Epstein and co-workers (1953):

$$t = 16.5 - 4.3\,(\delta_s - A) + 0.14\,(\delta_s - A)^2, \qquad (1)$$

where t is temperature, δ_s is the $\delta^{18}O$ value of the solid carbonate, and A is the $\delta^{18}O$ value of the water in which the carbonate precipitated, measured in the PDB system (Epstein and Mayeda, 1953; Epstein et al., 1953). The δ value is given as a proportional deviation of isotopic ratios from a standard:

$$\delta(m) = (R_m - R_s)/R_s,$$

where R is the ratio of the heavier to the lighter isotope, R_m denotes measured, and R_s denotes standard. The value for $\delta(m)$ is given in permil, that is, 1000 times the actual value of the deviation.

Term A in Equation 1 is a function mainly of the amount of water locked up in continental ice and the isotopic composition of that ice. Also, it contains information about fractionation processes involving evaporation and precipitation at the sea surface. These processes simultaneously influence salinity, so that an overall correlation exists between salinity and isotopic composition of seawater. The effect can be estimated and absorbed into the coefficient of slope in Equation 1, so that A then stands for the glacial effect alone (Berger and Mayer, 1987; Whitman and Berger, 1992). For this purpose, the slope coefficient in Equation 1 is set to 5.0, that is, a 1°C change in temperature produces a 0.2‰ change in the oxygen isotope ratio of foraminiferal tests. In the region studied here, we expect that the temperature range between glacials and interglacials is kept small by powerful feedback mechanisms involving evaporation and cloud shading (Ramanathan et al., 1989). From the pattern displayed in the CLIMAP reconstructions (CLIMAP Project Members, 1976), we assume that this range is about the same as the seasonal range, which is near 1°C. Thus, 0.2‰ of the 1.3‰–1.5‰ range observed for *G. sacculifer* may be ascribed to temperature, leaving 1.1‰–1.3‰ for other factors. An effect of differential dissolution on the range is likely, on the order of 0.1‰ to 0.2‰. This leaves between 1.1‰ and 1.2‰ for the range of the ice effect. Confidence in this assumption, of course, weakens as one proceeds backward into the record.

Depth Assignments

Depth assignments of samples are based on driller's depth and the distance of the sampling level from the core top within the recovered core (see ODP depths [given in mbsf], as listed in the individual site chapters of the *Initial Reports* volume). The ODP depths are adjusted by multiplying values for each core by a factor of <1.0 to account for excess recovery (>100%) and to make room for the gap postulated at the end of each core (estimated at 30 cm each; see below). This procedure results in an "adjusted" depth below seafloor (ambsf). For interpolation (5-cm intervals), records are first "filled in" to 2.5-cm intervals in the ODP scale, using estimates both from linear interpolation of adjacent measurements and from extrapolation of slopes from adjacent points. The final assignments are by straight line interpolation, between adjacent points of the artificially "filled-in" record ("resampling").

Age Assignments

Age assignments are based on Fourier analysis of the record of each core. Based on a preliminary estimate for the sedimentation rate of 17 m/m.y. (see Shipboard Scientific Party, 1991, "Site 805" chapter), the terms in the Fourier expansion that contain fluctuations in the vicinity of 41 k.y. (the period of obliquity oscillations in the Earth's axis) can be identified. These terms are then used to synthesize the apparent "obliquity response" in the sedimentary record. The resulting fluctuations are assigned a distance of 41 k.y. from peak to peak, which yields an estimate for the instantaneous sedimentation rate (ISR) within each meter of the section. A smooth curve is fit through these rates, using low-order Fourier terms. A summation of time intervals for successive depth intervals then yields an age for each depth in the core. No assumptions are made in the analysis beyond the one that the 41-k.y. obliquity cycle should be represented in the isotopic record. This assumption is abundantly supported by previous work (Hays et al., 1976; Pisias, 1976; Imbrie et al., 1984). Stability of the orbital signals seems assured for this interval (Berger, 1984). For details on the method, see the companion paper on Site 806 (Berger et al., this volume).

RESULTS AND DISCUSSION

Raw Data and Overview

Results of isotopic analyses are given in Table 1 and plotted in Figures 2A and 2B. The oxygen isotopes of *G. sacculifer* and *Pulleniatina* show the types of fluctuations, which are familiar from previous work on the plateau (Shackleton and Opdyke, 1973, 1976), with large amplitudes in Core 130-805C-1H, intermediate ones in Core 130-805C-2H, and rather small ones in Core 130-805C-3H. Also, typical wave lengths for the variations are seen to vary from about 1.5 m in Core 130-805C-1H to <1 m in Core 130-805C-3H, with a mixture of long and short waves in Core 130-805C-2H. This trend fits with previous findings that the late Quaternary record is dominated by a 100-k.y. cycle (eccentricity of Earth's orbit), and the early Quaternary by a much shorter cycle, corresponding to obliquity (Shackleton and Opdyke, 1976, 1977; Pisias and Moore, 1981; Ruddiman et al., 1986). The range in Core 130-805C-1H (late Quaternary) is near 1.5‰ (4 times standard deviation). If we assume 1° of temperature variation, this yields a range of 1.3‰ for non-temperature factors. Dissolution effects may be responsible, in part, for increasing this range over the equivalent one in Hole 806B during the same time interval (1.3‰ for 4 times standard deviation; Berger et al., this volume).

Typically, values of $\delta^{18}O$ are slightly more positive in Core 130-805C-1H than in Core 130-805C-3H; that is, the average ice mass is greater in the late Quaternary, or there is a cooling trend, or both. This trend is stronger in *Pulleniatina* than in *G. sacculifer*, suggesting that the thermocline tends to rise from early to late Quaternary (or that *Pulleniatina* changes its habitat to a deeper level, on average). Effects of differential dissolution may also enter into the equation: for increased dissolution, $\delta^{18}O$ values become more positive (Wu and Berger, 1989). Ranges of $\delta^{18}O$ values are substantially less in Core 130-805C-3H than in Cores 130-805C-2H and -1H. It appears that the long-wave effect (eccentricity) that arises in mid-Quaternary time may be considered an add-on to the short-wave effect (obliquity), so that the amplitude is correspondingly increased.

Table 1. Oxygen isotopes in *G. sacculifer* and *Pulleniatina*, Cores 130-805C-1H, -2H, and -3H.

Core, section	Depth (mbsf)	*G. sacculifer* neg $\delta^{18}O$ (‰, PDB)	*Pulleniatina* neg $\delta^{18}O$ (‰, PDB)
130-805C-			
1H-1	0.10	1.49	1.11
1H-1	0.20	1.52	0.90
1H-1	0.30	1.13	0.43
1H-1	0.40	1.04	0.68
1H-1	0.50	1.00	0.68
1H-1	0.60	1.17	0.87
1H-1	0.70	1.32	0.67
1H-1	0.80	1.22	0.89
1H-1	0.90	1.09	0.66
1H-1	1.00	0.66	0.44
1H-1	1.10	0.89	0.73
1H-1	1.20	1.30	0.87
1H-1	1.30	1.76	1.46
1H-1	1.40	1.51	0.92
1H-2	1.60	1.40	1.09
1H-2	1.70	1.85	1.06
1H-2	1.80	1.74	1.03
1H-2	1.90	1.57	0.62
1H-2	2.00	0.84	0.09
1H-2	2.10	0.72	0.25
1H-2	2.20	0.80	0.34
1H-2	2.30	0.82	0.19
1H-2	2.40	0.88	
1H-2	2.50	0.91	0.74
1H-2	2.60	0.87	0.77
1H-2	2.70	0.76	0.57
1H-2	2.80	1.07	0.70
1H-2	2.90	1.60	1.16
1H-2	2.99	1.48	0.77
1H-3	3.10	1.42	0.78
1H-3	3.20	1.20	0.97
1H-3	3.30	1.15	0.71
1H-3	3.40	1.36	1.17
1H-3	3.50	1.53	0.86
1H-3	3.60	0.92	0.68
1H-3	3.70	0.88	0.31
1H-3	3.80	1.05	0.64
1H-3	3.90	0.87	0.57
1H-3	4.00	0.81	0.29
1H-3	4.10	0.56	0.50
1H-3	4.20	1.43	0.89
1H-3	4.30	1.40	0.91
1H-3	4.40	1.29	0.67
1H-3	4.49	1.16	0.88
1H-4	4.60	1.33	1.14
1H-4	4.70	1.27	0.91
1H-4	4.80	1.28	1.09
1H-4	4.90	1.20	1.13
1H-4	5.00	1.42	0.85
1H-4	5.10	1.31	0.09
1H-4	5.20	1.06	0.04
1H-4	5.30	0.60	0.10
1H-4	5.40	0.70	0.21
1H-4	5.50	0.41	0.32
1H-4	5.60	0.73	
1H-4	5.70		
1H-5	6.10	1.69	1.31
1H-5	6.20	1.46	1.29
1H-5	6.30	1.37	
1H-5	6.40	1.00	−0.11
1H-5	6.50	0.57	0.03
1H-5	6.60	0.50	−0.10
1H-5	6.70	0.12	−0.19
1H-5	6.80	0.38	0.09
1H-5	6.90	0.66	0.32
1H-5	7.00	0.58	0.31
1H-5	7.10	0.51	0.48
1H-5	7.20	0.92	0.51
1H-5	7.30	1.08	0.62
1H-5	7.40	0.46	0.96
1H-5	7.49	1.26	0.96
2H-1	0.10	0.72	0.63
2H-1	0.20	1.25	1.02
2H-1	0.30	1.29	1.30
2H-1	0.40	1.26	1.22
2H-1	0.50	1.42	1.23
2H-1	0.60	1.39	1.15
2H-1	0.70	1.76	1.24
2H-1	0.80	1.37	1.26
2H-1	0.90	1.37	0.85
2H-1	1.00	1.11	0.85
2H-1	1.10	1.41	0.99
2H-1	1.20	1.19	0.89
2H-1	1.30	1.37	0.96
2H-1	1.40	1.42	1.17
2H-1	1.49	1.35	0.27
2H-2	1.60	1.31	1.12
2H-2	1.70	1.29	1.02
2H-2	1.80	0.52	0.17
2H-2	1.90	0.52	0.08
2H-2	2.00	0.18	−0.17
2H-2	2.10	0.39	0.12
2H-2	2.20	0.47	0.14
2H-2	2.30	0.69	0.18
2H-2	2.40	0.52	0.40
2H-2	2.50	0.85	0.36
2H-2	2.60	0.45	0.34
2H-2	2.70	0.63	0.26
2H-2	2.80	0.57	0.58
2H-2	2.90	0.76	0.23
2H-2	2.99	0.63	0.28
2H-3	3.10	1.03	0.48
2H-3	3.20	0.75	0.20
2H-3	3.30	0.90	0.72
2H-3	3.40	1.19	1.06
2H-3	3.50	1.28	1.04
2H-3	3.60	1.10	0.90
2H-3	3.70	1.06	0.56
2H-3	3.80	0.59	0.48
2H-3	3.90	0.61	0.47
2H-3	4.00	1.07	0.59
2H-3	4.10	1.11	0.94
2H-3	4.20	0.93	0.63
2H-3	4.30	0.86	0.57
2H-3	4.40	1.43	0.49
2H-3	4.49	0.79	−0.28
2H-4	4.60	0.90	0.84
2H-4	4.70	1.25	1.08
2H-4	4.80	1.32	1.23
2H-4	4.90	1.40	1.12
2H-4	5.00	0.95	0.57
2H-4	5.10	0.83	
2H-4	5.20	0.46	0.24
2H-4	5.30	0.70	0.60
2H-4	5.40	0.73	0.59
2H-4	5.50	0.98	0.74
2H-4	5.60		
2H-4	5.70	1.48	1.07
2H-4	5.80	1.33	1.04
2H-4	5.90	1.26	1.08
2H-5	6.10	1.43	1.03
2H-5	6.20	1.15	1.22
2H-5	6.30	1.22	1.21
2H-5	6.40	0.72	0.47
2H-5	6.50	0.76	0.13
2H-5	6.60	0.74	0.40
2H-5	6.70	0.68	0.32
2H-5	6.80	0.63	0.29
2H-5	6.90	0.78	0.64
2H-5	7.00	1.06	0.79
2H-5	7.10	1.01	0.74
2H-5	7.20	0.91	0.78
2H-5	7.30	0.71	0.42
2H-5	7.40	0.76	0.57
2H-6	7.60	1.11	0.87
2H-6	7.70	1.16	1.23
2H-6	7.80	1.36	1.08
2H-6	7.90	1.17	1.25
2H-6	8.00	1.31	1.20
2H-6	8.10	1.25	1.27
2H-6	8.20	1.18	0.94
2H-6	8.30		0.84
2H-6	8.38	0.43	0.16
2H-6	8.42	0.43	0.16
2H-6	8.50		0.32
2H-6	8.60	0.97	0.67
2H-6	8.70	1.17	
2H-6	8.80	1.12	0.87
2H-6	8.90	1.29	0.97
2H-6	8.99	0.89	0.68
2H-7	9.10	1.19	0.76
2H-7	9.20	1.27	0.98
2H-7	9.30	1.05	0.94
2H-7	9.40	1.22	0.97
2H-7	9.50	1.20	0.68
2H-7	9.60	1.10	0.99
2H-7	9.70	1.37	1.07
3H-1	0.10	1.33	1.01
3H-1	0.20	1.26	1.02
3H-1	0.30	0.90	1.00
3H-1	0.40	1.08	0.65
3H-1	0.50	0.71	0.94
3H-1	0.60	0.82	0.44
3H-1	0.70	1.09	1.08
3H-1	0.80	1.32	1.07
3H-1	0.90	1.25	0.93
3H-1	1.00	1.23	1.05
3H-1	1.10	1.16	0.91
3H-1	1.20	0.64	0.34
3H-1	1.30	0.96	0.49
3H-1	1.40	0.82	0.67
3H-2	1.60	1.20	0.67
3H-2	1.70	1.36	1.09
3H-2	1.80		
3H-2	1.90	1.27	0.85
3H-2	2.00	1.20	0.88
3H-2	2.10	0.98	0.41
3H-2	2.20	0.72	0.41
3H-2	2.30	1.07	0.95
3H-2	2.40	1.18	0.97
3H-2	2.50	1.26	1.16
3H-2	2.60	1.24	0.88
3H-2	2.70	1.02	0.82
3H-2	2.80	1.18	0.84
3H-2	2.90	0.82	0.59
3H-2	2.99	1.04	0.94
3H-3	3.10	1.27	0.95
3H-3	3.20	1.31	1.01
3H-3	3.30	1.23	0.81
3H-3	3.40	1.05	0.90
3H-3	3.50	1.00	0.86
3H-3	3.60	0.96	0.63
3H-3	3.70	1.14	0.76
3H-3	3.80	1.23	1.05
3H-3	3.90	1.54	1.18
3H-3	4.00	1.32	1.16
3H-3	4.10	1.21	0.87
3H-3	4.13	1.26	0.67
3H-3	4.30	1.06	0.64
3H-3	4.40	1.17	0.76
3H-3	4.49	1.27	1.10
3H-4	4.60	1.45	1.00
3H-4	4.70	1.12	0.88
3H-4	4.80	1.10	0.86
3H-4	4.90	1.01	
3H-4	5.00		
3H-4	5.10		1.19
3H-4	5.20		1.11
3H-4	5.30	1.46	1.10
3H-4	5.40	1.63	1.30
3H-4	5.50	1.49	1.05
3H-4	5.60	0.92	0.80
3H-4	5.70	1.03	0.45
3H-5	6.10	1.33	1.15

Table 1 (continued).

Core, section	Depth (mbsf)	*G. sacculifer* neg $\delta^{18}O$ (‰, PDB)	*Pulleniatina* neg $\delta^{18}O$ (‰, PDB)
3H-5	6.20	1.16	1.09
3H-5	6.30	1.22	0.62
3H-5	6.40	0.92	0.73
3H-5	6.50	1.19	1.15
3H-5	6.60	1.08	
3H-5	6.70	1.36	0.92
3H-5	6.80	1.17	0.86
3H-5	6.90	0.87	0.72
3H-5	7.00	0.75	0.56
3H-5	7.10	1.00	0.91
3H-5	7.20	1.35	0.91
3H-5	7.30	1.25	0.85
3H-5	7.40	1.07	0.75
3H-5	7.49	1.22	0.77
3H-6	7.60	0.96	0.74
3H-6	7.70	1.15	0.87
3H-6	7.80	1.22	0.97
3H-6	7.90	1.23	1.25
3H-6	8.00	1.01	0.97
3H-6	8.10	1.35	0.91
3H-6	8.20	1.15	0.90
3H-6	8.30	1.31	0.86
3H-6	8.40	1.36	1.10
3H-6	8.50	1.04	1.03
3H-6	8.60	1.14	0.70
3H-6	8.70	0.78	0.67
3H-6	8.80	1.11	0.68
3H-6	8.90	0.87	0.67
3H-6	8.99	1.09	0.75
3H-7	9.10	1.22	0.77
3H-7	9.19	1.18	0.95

Notes: Depths are uncorrected official ODP values (Kroenke, Berger, Janecek, et al., 1991). Oxygen isotopes are given as negative $\delta^{18}O$‰ (deviation from PDB standard).

DEPTH MODEL AND DEPTH SERIES

General

The depths given for the raw data (Figs. 2A and 2B) are the ODP depths, which are based on counting core barrels, by the driller, and on measuring depth-in-core after retrieval (mbsf). It is to be expected that there might be gaps between cores as well as an overlap between adjacent cores, because of core expansion on deck. To obtain a best estimate for depth below seafloor for each sample, we make the following assumptions:

1. The top of the sediment in the first core is taken as 0.0 mbsf.
2. The top of all other cores is the driller's depth (ODP depth).
3. Cores must not overlap; thus, the minimum gap between the last sample of one core and the first sample in the next below is the distance of the two samples that appears when the bottom of the first core is laid flush against the top of the second. This is the *sampling gap.*
4. A *coring gap* is expected; it must be deduced by (a) matching properties of multiple cores (with breaks at different horizons), or (b) matching of properties with an idealized profile, or some other profile based on expectations from previous work.

We have used two methods to find any coring gaps: (1) the matching of the $\delta^{18}O$ record of Hole 805C with those of Cores V28-238 and V28-239, from the same area (published by Shackleton and Opdyke, 1973, 1976); and (2) a visual comparison of gamma-ray attenuation porosity evaluator (GRAPE) data for Holes 805A, 805B, and 805C, as taken on board (kindly provided by T.R. Janecek). The attempt at matching patterns of GRAPE series turned out to be unconvincing, because correlations between the parallel cores are not consistently obvious. However, GRAPE data do support our results from matching with the Vema records: all estimates for the coring gaps (Cores 1H to 2H, 2H to 3H, and 3H to 4H) came to within a few centimeters of 30 cm. Hence, this is the estimate we use here. Derivation of the gap size is summarized in Table 2.

Once a gap has been identified, it needs to be filled in with estimates of isotopic values, so that evenly spaced series can be extracted from the record for analysis. Straight-line interpolation between the boundaries of the gap is unattractive. This becomes obvious when the points at the edges are unusually high or low. In the absence of other information, it is more reasonable to assume that there will be two factors allowing extrapolation from the edges into the gap: a tendency for continuation of an established trend on approaching the gap, and a tendency to return toward the mean. The records treated here have strong cyclic elements and are autocorrelative at a shift of around 200 k.y. (two eccentricity cycles and five obliquity cycles). This autocorrelation is useful when guessing missing values within coring or sampling gaps. In filling gaps, we have used these three methods (continuity of trend, return to average, and autocorrelation) with roughly equal weight. We eschewed more sophisticated mathematical techniques as needless complications that provide a false sense of security. It is well to remember that, whatever the approach, the filling of gaps is strictly guesswork. We intend to improve on these estimates in the future by additional sampling and splicing from other records.

Match Between Hole 805C and Core V28-238

Hole 805C was drilled at a depth of 3188 m, and Core V28-238 was taken at 3120 m, only a few miles away. Thus, one would expect an excellent match between the two records. On the whole, this expectation is fulfilled (Fig. 3). The match suggests, however, that one of the two cores is disturbed within certain intervals. We think that the more reliable stratigraphy of the two cores is the one from Hole 805C.

The match between the two cores (Fig. 3) shows the original record of Core V28-238 on top (with a linear depth-scale transform), and the adjusted record on the bottom (V28-238 altered). The record of Hole 805C represents the $\delta^{18}O$ stratigraphy for Cores 130-805C-1H and -2H, with the gap (coring plus sampling) filled as shown. The ODP depths for Core 130-805C-1H were multiplied by 0.96 to obtain room for the gap (and to take account of excess recovery). Measured depths within Core 130-805C-2H were multiplied by 0.93 and added to 7.80 mbsf (the driller's depth for the core top). The Brunhes/Matuyama boundary in Hole 805C (ODP depth, 12.7 mbsf; Shipboard Scientific Party, 1991) then appears at 12.36 mbsf, as shown. The sampling depths given for Core V28-238 were consequently multiplied by a factor of 1.03 (i.e., 12.36/12.00) to adjust for the difference in depth for this boundary (12 m in V28-238).

One can see that the numbered isotope stages of Core V28-238 are readily matched to the corresponding excursions in the record of Hole 805C. However, compared with Hole 805C, the section down to Stage 13 seems expanded (especially so for Stage 11), and the section between Stages 15 and 19 seems greatly reduced. The mismatch around Stage 11 is addressed by Prell et al. (1986, p. 149), who note that the section around Stage 11 in Core V28-238 was disturbed by uncoupling of the core pipes. Some disturbance is also postulated for the structure within Stage 5, from the same process, "when the core was extruded." Presumably, similar disturbances may exist in other portions of this core. Visual comparison of the normalized stratigraphy of nearby Core RC17-177 with that of Core V28-238 (given in Prell et al., 1986, in fig. 9) suggests that Stages 13 and 15 are correctly represented in Core V28-238 (as is necessary if we are to use this record for finding the gap in Hole 805C), but that Stage 17 is indeed underrepresented (as suggested by the match in Fig. 3).

The record at the bottom of Figure 3 represents the $\delta^{18}O$ stratigraphy of Core V28-238, adjusted for a fit to the one of Hole 805C. The adjustment was made by expanding and compressing 1-m sections of

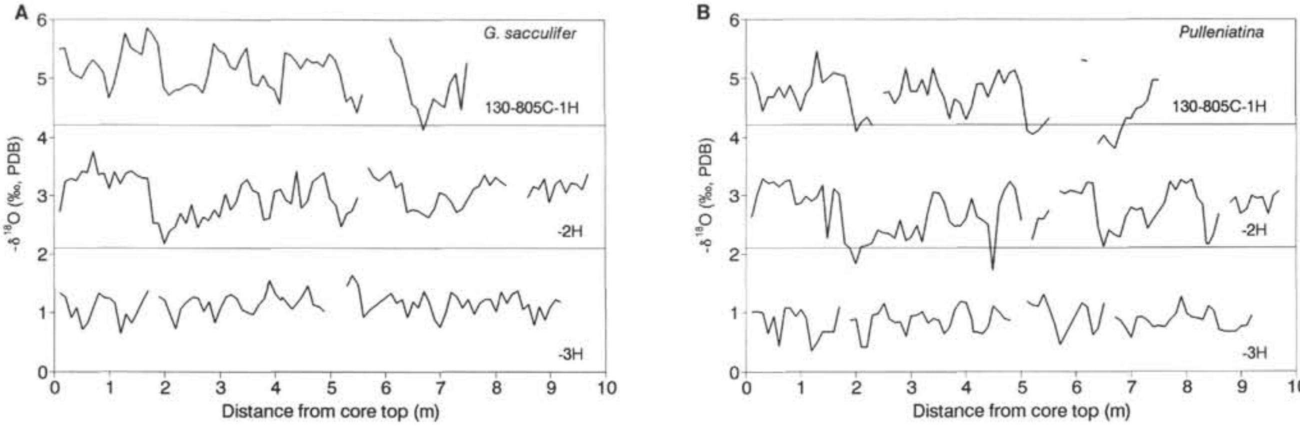

Figure 2. Oxygen isotope records of *G. sacculifer* (**A**) and *Pulleniatina* (**B**), raw data. Gaps are shown where the distance between samples is >15 cm.

Table 2. Depth-related parameters (in meters) for Cores 130-805C-1H to -3H.

Core	1H	2H	3H
Length cored	7.80	9.50	9.50
Recovered	7.80	9.88	9.40
ODP depths	0–7.8	7.8–17.3	17.3–26.8
First sample	0.10	0.10	0.10
Last sample	7.49	9.70	9.19
Sampling gap	0.31 + 0.1	0.18 + 0.1	0.21 + 0.1
Coring gap (V28)	0.25	0.37	n.d.
Coring gap (GRP)	0.36	0.32	0.30
Factor	0.96	0.93	0.98
Accepted coring gap	0.30	0.30	0.30
Adjusted depth	0–7.5	7.8–17.0	17.3–26.5

Note: Also see note added in proofs after "Acknowledgments" section (this chapter).

the original record shown on top. The corresponding factors represent a series of sedimentation rate ratios (SRR), which are plotted in Figure 4. The ratio starts at 1.2 at the top and drops to near 1 below the Brunhes/Matuyama boundary. Distinct excursions occur within Stages 6 and 11, in rough agreement with the disturbances identified by Prell et al. (1986). An excursion to low values within Stage 16 is present, which suggests yet another disturbance in the record of Core V28-238.

In summary, the match with Core V28-238 allows identification of a gap of about 30 cm between Cores 130-805C-1H and -2H, and also allows assignment of isotope stages. Two out of three discrepancies between the two cores are identified as probable disturbances in Core V28-238. The question of whether Stage 16 is undersampled in Core V28-238 or oversampled in Hole 805C is addressed below.

To find the gap between Cores 130-805C-2H and -3H, and to further document the nature of discrepancies between the records of Hole 805C and Core V28-238, we next match the stratigraphies of Hole 805C and Core V28-239 (as given in Shackleton and Opdyke, 1976) (Fig. 5). The procedure is that described for Figure 3. The linear adjustment of the depths of Core V28-239, by correlation to the Brunhes/Matuyama boundary, produces an excellent fit with Hole 805C down to Stage 17. Stage 19 is reduced or missing in Core V28-239; this is the stage that has the Brunhes/Matuyama (B/M) boundary. Stage 21 also seems reduced in Core V28-239, whereas Stage 23 is well represented. Stretching the Core V28-239 record below the Brunhes/Matuyama boundary to make it fit the oxygen isotope record of Hole 805C (bottom series) also brings in line the Matuyama/Jaramillo boundary positions.

The relationships between the two stratigraphies are plotted in Figure 6 as instantaneous sedimentation rate ratios. Core V28-239 comes from a depth of 3490 m and is well off the equator (3°15′N). Thus, its sedimentation rate is lower than that of Hole 805C and the SRR is below 1. It starts near 0.7 at the top, decreases toward the Matuyama/Jaramillo boundary, rises to a little over 0.8 below that, and drops again below 14 m in the core. There are two major downward excursions. The first, going down in Core V28-239, is at Stage 11. This is the reverse of the situation in Core V28-238. Thus, Hole 805C represents the intermediate (and most likely true) condition. The second excursion, which is quite large, is in the vicinity of the Brunhes/Matuyama boundary. Also, one can see that no anomaly is present at Stage 16, so that the records of Core V28-239 and Hole 805C agree that this section is underrepresented in Core V28-238.

In summary, when comparing the SRR anomalies of Core V28-238/Hole 805C and Core V28-239/Hole 805C, one can see that their patterns are not similar, which would be the case if Hole 805C had the odd record. This supports our contention that the depth model for Hole 805C is essentially correct, and that its stratigraphy is more reliable than that of either of the Vema cores.

AGE MODEL AND TIME SERIES

Dating by Counting Obliquity Cycles: *G. sacculifer* Record

The assignment of ages, as mentioned, is based on the counting of $\delta^{18}O$ cycles of approximately 40-k.y. length (i.e., typically 60–80 cm wavelength in the cored sequence). Equally spaced $\delta^{18}O$ values were obtained by first filling in between adjacent samples using a weighted mean of three estimates: the mid-point of the straight-line interpolation, and two values derived from extrapolating the trends from the two points preceding the new position and the two following it. Giving the first estimate 4.5 times the weight of the others results in a smooth sinusoidal fit. This new curve is then resampled at 5-cm intervals by straight-line interpolation. The Fourier components of the series were determined separately for three sections: (1) the late Quaternary or "Milankovitch Regime," in which eccentricity cycles dominate; (2) the middle Quaternary or "Croll Regime," in which both eccentricity and obliquity are important, and (3) the early Quaternary or "Laplace Regime," in which obliquity cycles dominate entirely. The terms are chosen for historic and mnemonic reasons (Berger and Wefer, in press).

The Milankovitch Regime is defined as the sequence from the present back to $\delta^{18}O$ Stage 15 (or, more precisely, the crest of the 15th obliquity cycle, counting the last crest as zero) (Fig. 7). The top of the record was extended by shifting the last 200 k.y. forward into the future. The appendix is linearly tapered toward the mean, at 200 k.y. into the future (not shown). The assumed sedimentation rate is 1.4 cm/k.y. The appendix at the end of the series was formed in analogous fashion. Figure 7 shows the extended record, a Fourier fit

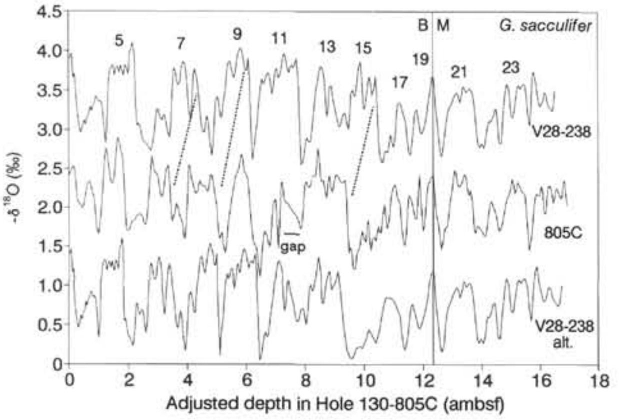

Figure 3. Comparison of $\delta^{18}O$ stratigraphies of Hole 805C (this study) and Core V28-238 (Shackleton and Opdyke, 1973). Scales shifted for clarity. Top, depth in Core V28-238 adjusted linearly to that in Hole 805C (factor = 1.03). Bottom, depth in Core V28-238 altered by mapping its $\delta^{18}O$ signal onto that of Hole 805C, at 1-m intervals. Isotope stages are as given in Shackleton and Opdyke (1973).

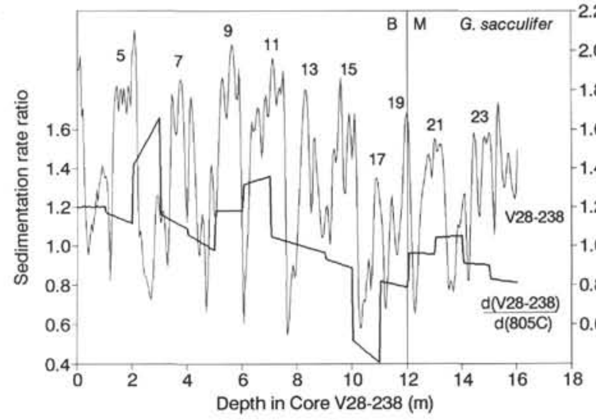

Figure 4. Instantaneous sedimentation rate ratios between Core V28-238 and Hole 805C (d[V28-238]/d[805C]), based on the fit of $\delta^{18}O$ stratigraphies shown in Figure 3 (V28-238 altered). The record of Core V28-238 (SMOW scale on right) is given for identification of positions of discrepancies. Upward excursions indicate expansion relative to Hole 805C; downward excursions indicate reduction of equivalent sections.

derived from the main 12 harmonics (in essence, a smoothed version of the original curve), an eccentricity-related component, and an obliquity-related component, all offset from each other for clarity.

The Fourier fit demonstrates that relatively few harmonics represent most of the information contained in the record. The eccentricity-related component is represented by Harmonics 8 through 12 of a record that is 1375 cm long; that is, it contains the cycles with wavelengths between 170 and 110 cm, approximately. This range is set to contain the eccentricity signal for sedimentation rates between 1.1 and 1.7 cm/k.y. Recognition of the dated Stage 5e (see Shackleton and Opdyke, 1973) yields a first guess for the sedimentation rate between 1.3 and 1.4 cm/k.y. Eccentricity Cycle 6 ("E6") is seen to coincide with Stage 15. Thus, the Milankovitch Regime is somewhat longer than 600 k.y.

For detail, we turn to the obliquity record (Harmonics 20 to 30, corresponding to wavelengths of about 70–45 cm, for assumed sedimentation rates between 1.7 and 1.1 cm/k.y.). We see that the sharp transition at the beginning of Stage 15 is due to the presence of the crest of obliquity Cycle 15 ("o15"). The time interval from this point to the top of the core is 15×41 k.y. + 15 k.y., which is 630 k.y. The interval indicated by counting eccentricity cycles is similar: about 625 k.y. In Hole 806B the equivalent level was found as 623 ka (Berger et al., this volume). Both determinations agree well with that given in the SPECMAP model (617 ka; Imbrie et al., 1984) (although at greater depths our scale begins to deviate markedly from SPECMAP). Here we take the end of the transition between Stages 16 and 15 as 630 yr, and this then is the duration of the Milankovitch Regime based on the present data set.

A similar analysis is next made for the Croll Regime (Fig. 8). It is defined as the interval between o15 and o30; that is, it is 615 k.y. long. For this series, extensions were taken from the adjacent sections and tapered linearly toward the mean at the ends. The eccentricity-related component weakens considerably in the early part of the Croll Regime. Stage 23, in the middle of the Croll section, is seen to be about 1 m.y. old, as it coincides with E10. It also coincides with o23, which yields an age of $8 \times 41 + 630$, that is, 958 ka. The discrepancy is 42 ka, or one obliquity cycle. If we count the blip showing below o16 in the bottom curve of Figure 8, this discrepancy disappears. If we do not count the subdued eccentricity cycle below E7, another discrepancy arises. Thus, we could reasonably adjust the count by adding one obliquity cycle.

There is one important problem with this adjustment, however. Recall that the Brunhes/Matuyama boundary intersects the main peak

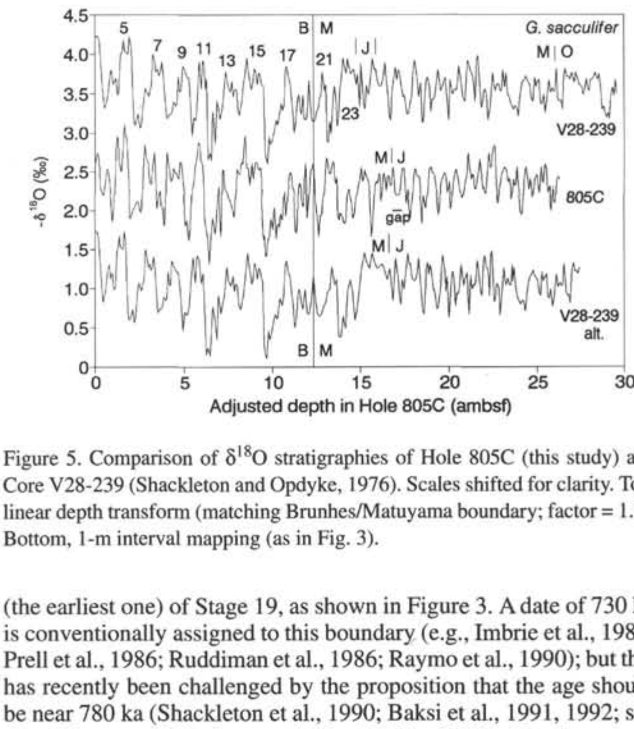

Figure 5. Comparison of $\delta^{18}O$ stratigraphies of Hole 805C (this study) and Core V28-239 (Shackleton and Opdyke, 1976). Scales shifted for clarity. Top, linear depth transform (matching Brunhes/Matuyama boundary; factor = 1.7). Bottom, 1-m interval mapping (as in Fig. 3).

(the earliest one) of Stage 19, as shown in Figure 3. A date of 730 ka is conventionally assigned to this boundary (e.g., Imbrie et al., 1984; Prell et al., 1986; Ruddiman et al., 1986; Raymo et al., 1990); but this has recently been challenged by the proposition that the age should be near 780 ka (Shackleton et al., 1990; Baksi et al., 1991, 1992; see also Johnson, 1982; Izett and Obradovich, 1991). The lesser age would put Stage 19 just above o18 in the section. The greater age would correlate it exactly with o19. If we count the blip below o16 as a cycle, we would then arrive at o20 for correlation with Stage 19, assigning an age of 830 ka to the Brunhes/Matuyama boundary. This age is well outside the range of values previously proposed. For present purposes, we shall ignore the blip and count as shown. This puts the Brunhes-Matuyama boundary into o19, for an age of 4×41 + 630 (i.e., 794 ka), in good agreement with the preference of Shackleton et al. (1990) and with the age model for Hole 806B (Berger et al., this volume).

Nevertheless, it is unsatisfactory that o23 should coincide with E10, because this implies that the usual phase relationships between the major cycles are not valid in this vicinity. In other words, Stages 19, 21, and 23 do not fit the pattern seen in the more regular

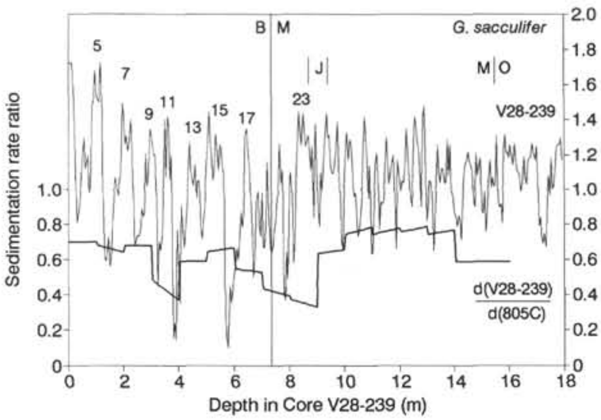

Figure 6. Instantaneous sedimentation rate ratios between Core V28-239 and Hole 805C (d[V28-239]/d[805C]), based on the fit of $\delta^{18}O$ stratigraphies shown in Figure 5. The record of Core V28-239 is given for identification of positions of discrepancies (PDB scale on right). Upward excursions indicate expansion relative to average ratio to equivalent sections in Hole 805C; downward excursions indicate reduction.

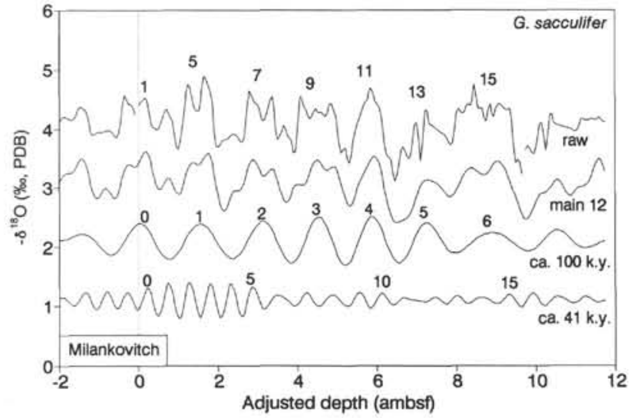

Figure 7. Fourier analysis of the upper Quaternary portion of the $\delta^{18}O$ record of *G. sacculifer* in Hole 805C, extended by shifting autocorrelated ends and tapered (see text). Milankovitch Regime: last 15 obliquity cycles. "Main 12" refers to dominant harmonics.

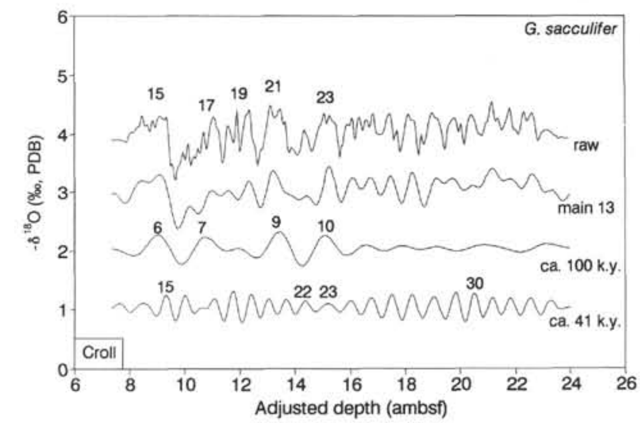

Figure 8. Fourier analysis of the middle Quaternary portion of the $\delta^{18}O$ record of *G. sacculifer* in Hole 805C, extended by shifting ends and tapered (see text). Croll Regime: period between 15th and 30th obliquity cycle. "Main 13" refers to dominant harmonics.

Milankovitch Regime. The discrepancy arises because E8 is so poorly expressed, which in turn is due to the fact that Stage 18 is weak and short. The composite $\delta^{18}O$ record of Prell et al. (1986) suggests that this is generally true and not just peculiar to the record of Hole 805C. The possibility that the proposed age of the Brunhes/Matuyama boundary, at 794 ka, is still too young by one obliquity cycle cannot be discounted. The date for this boundary has seen many reevaluations for the last 20 yr toward higher values.

Fourier analysis of the Laplace Regime, defined as the interval between o30 and o45, demonstrates the dominance of the obliquity cycles, and the absence, in essence, of eccentricity cycles (Fig. 9). The available series is seen to bottom in o39; self-similarity was used to append the extension, which was tapered to avoid edge effects in the Fourier components. The range of harmonics used for synthesis of eccentricity- and obliquity-related variations ("window") was 7 to 12 and 19 to 30, respectively, as before.

Results of the counting exercise are summarized in Figure 10 for ready reference. Counting of traditional isotope stages, in the odd-even scheme introduced by Emiliani (1955), ends with Stage 23 (Shackleton and Opdyke, 1976). We have not attempted to label older stages by comparing with other stratigraphies (Ruddiman et al., 1986; Shackleton et al., 1990; Raymo et al., 1990), because such correlation requires careful matching of biostratigraphic information. (The necessary data are now available through the detailed investigations of T. Takayama [this volume], so that these comparisons will be possible in the near future.) Instead, we have used the regular sequence of obliquity cycles, which allows instant conversion to an age estimate. The point at which the crest of each cycle appears is dated relative to Obliquity Crest 0, which is the very first crest just below the core top ("o0"). The time interval from o0 to the top is found by extrapolating the sedimentation rate between o0 and the next deeper crest ("o1") toward the top of the core.

How reliable is our method of dating? There are several ways to approach this question: internal consistency within the same record (comparison of eccentricity- and obliquity-related signal), comparison with results from another record within the same core, and comparison with other cores. We have mentioned the good agreement with the SPECMAP age model back to Stage 15. Also, we have referred to internal consistency earlier and found it somewhat lacking in the vicinity of the Brunhes/Matuyama boundary. Apparently, in the interval of transition to a dominance of major eccentricity cycles, the system does not behave in the highly regular fashion that is apparent before and after this period.

We next compare the results so far obtained by a similar analysis for the $\delta^{18}O$ record of *Pulleniatina*, to further check on reliability.

Dating by Counting Obliquity Cycles: *Pulleniatina* Record

The procedure of analysis is the same as that for *G. sacculifer:* Figs. 11, 12, and 13 correspond to Figs. 7, 8, and 9, respectively. In the Milankovitch portion (Fig. 11), the most striking aspect is again the dominance of the eccentricity-related cycles. There is a problem in Stage 15: both the 100 and 41 k.y. windows show poor fit to the data. Apparently, Stage 15 is too broad for a good fit; that is, the transition from Stage 16 to Stage 15 starts too early or is otherwise irregular. The Croll portion (Fig. 12) pretty much repeats the picture seen in the *G. sacculifer* record—again, there is the mismatch between E10 and o23, and the "blip" below o16 that, if counted as a cycle, would remove the discrepancy. In the Laplace section of the *Pulleniatina* record, the eccentricity-related cycles are slightly greater than those seen in *G. sacculifer,* but they still have very little power.

The summary graph for obliquity counting in the *Pulleniatina* $\delta^{18}O$ record (Fig. 14) is rather similar to the one for *G. sacculifer* (Fig. 10). Stage 23 is seen to correspond to o23, and the record terminates just before o38, within o39.

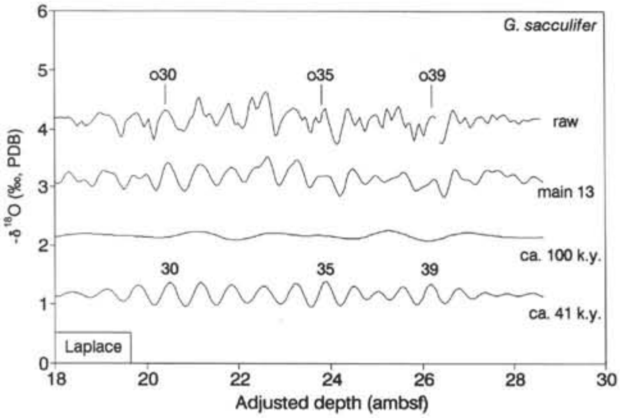

Figure 9. Fourier analysis of the lower Quaternary portion of the $\delta^{18}O$ record of *G. sacculifer* in Hole 805C, extended by shifting ends and tapered (see text). Laplace Regime: period between 30th and 45th obliquity cycle. "Main 13" refers to dominant harmonics.

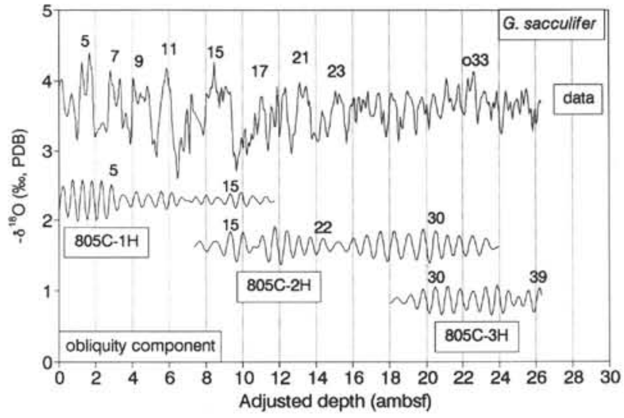

Figure 10. Summary of obliquity cycle counting in the $\delta^{18}O$ record of *G. sacculifer* in Hole 805C, down to obliquity cycle 39. "o33" = crest of 33rd obliquity cycle. (The most recent crest is defined as zero.)

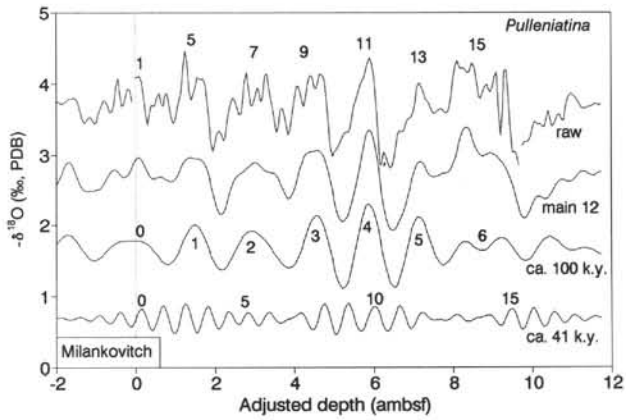

Figure 11. Fourier analysis of the upper Quaternary portion of the $\delta^{18}O$ record of *Pulleniatina* in Hole 805C (Milankovitch Regime). Compare with Figure 7.

A detailed comparison of the results of obliquity dating for the two records emerges when plotting instantaneous sedimentation rates (ISR) on top of each other (Fig. 15). Over much of the sequence the agreement is excellent. Sedimentation rates typically vary between 1.3 cm/k.y. near the top of the core and 2 cm/k.y. in the middle Quaternary. Low values are shown in the vicinity of the Brunhes/Matuyama boundary. The lower Quaternary shows somewhat lower ISR values in both records. However, a section with major discrepancies is present in the vicinity of Stages 13 to 15. The section of greatest disagreement coincides with the break between Cores 130-805C-1H and -2H; this may account for much of the problem. However, there is strong disagreement also at the beginning of Stage 15, which is well below the break.

Age Assignments and Age Model

There seems to be no good reason to prefer the estimates of instantaneous sedimentation rate results of one taxon over that from the other; therefore, for the subsequent age assignment, we have taken the average of the two independent ISR determinations.

Using this average of the smooth curves shown in Figure 15, we can now assign an age to each position in Hole 805C. We did this at 5-cm steps, and then we resampled at intervals of 4 k.y. by straight-line interpolation (see Table 3). The resulting curves represent the age model for Cores 130-805C-1H through -3H (Fig. 16).

The entire sequence was then analyzed once again in the time domain (Fig. 17). The windows are set at 87–118 k.y. and 36–47 k.y., that is, about 15% beyond either side of the expected periods. The results confirm in some detail what has emerged already: (1) the excellent agreement between the records of *G. sacculifer* and *Pulleniatina;* (2) the dominance of the eccentricity-related cycle in the interval since o15 (Milankovitch Regime); (3) the dominance of obliquity-related fluctuations in the interval below o27 (lowermost Croll and Laplace regimes); and (4) the transitional interval between o27 and o15 (most of the Croll Regime). The irregularity of the interval in the vicinity of Stages 17 to 19 is reflected in the apparent phase reversal of the eccentricity-related cycles.

The fact that the eccentricity-related cycles are not entirely "clean" is also seen in the Fourier spectrum (Fig. 18). The 100-k.y. peak has a lesser but distinct adjunct to the right (higher harmonic), which produces an interference pattern. The 41-k.y. peak, naturally, is strong and distinct as a result of our procedure. The *Pulleniatina* record has a Fourier peak near 30 ka, which is absent from the *G. sacculifer* record. Power within the band corresponding to precession (19 and 23 k.y.) is but slightly elevated over background: the present analysis presents no evidence on the importance of precession in these records.

COMPARISON OF OXYGEN ISOTOPE RECORDS WITHIN HOLE 805C

Eccentricity Domain

We have noted earlier, when discussing Figures 2 and 3, that the $\delta^{18}O$ records of *G. sacculifer* and *Pulleniatina* show certain differences that change through time. In Core 130-805C-1H, the $\delta^{18}O$ values of the two taxa differ by 0.42‰ on average, in Core 130-805C-2H by 0.29‰, and in Core 130-805C-3H by 0.27‰. Thus, there is an increase in difference with time within the Quaternary. Also, the amplitude of the $\delta^{18}O$ fluctuations increases: from 0.8‰ in Core 130-805C-3H to ca. 1.5‰ in Cores 130-805C-2H and -1H. Could there be a relationship between these two trends? Differential dissolution decreases the contrast between $\delta^{18}O$ values of *G. sacculifer* and *Pulleniatina* (Wu and Berger, 1989). Thus, the relatively smaller contrast in Core 130-805C-2H, despite higher overall amplitudes, may in part be due to increased dissolution effects in that core.

Before such questions can be properly attacked, the actual patterns of the relationships between the $\delta^{18}O$ records of the two taxa must be established in some detail. In the following, we derive average patterns over one eccentricity cycle by summing the relevant variables *modulo* 100 k.y.; that is, we "stack" successive eccentricity cycles

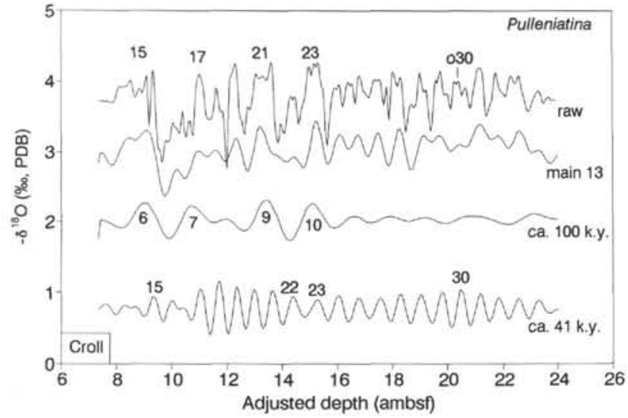

Figure 12. Fourier analysis of the middle Quaternary portion of the $\delta^{18}O$ record of *Pulleniatina* in Hole 805C (Croll Regime). Compare with Figure 8.

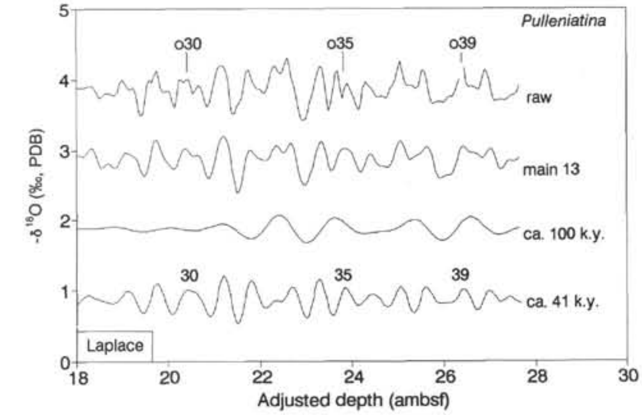

Figure 13. Fourier analysis of the lower Quaternary portion of the $\delta^{18}O$ record of *Pulleniatina* in Hole 805C (Laplace Regime). Compare with Figure 9.

("autostacking"). Each "autostack" consists of the average of five consecutive intervals.

The first such autostack, from 0 to 500 ka, shows a distinct cycle, as expected (Fig. 19A). The peak appears at 20 to 30 ka for both *G. sacculifer* ("SOX") and *Pulleniatina* ("POX"). Because the two curves do not line up exactly, the difference varies: it is greatest in the early phase of the transition from glacial to postglacial condition ("deglaciation," 70–30 ka) and lowest during the transition from the interglacial to the glacial condition ("reglaciation," 100–70 ka). The sense of the difference variation is as expected, if dissolution plays a role. During deglaciation preservation increases, and hence the original isotopic difference is preserved. During reglaciation a dissolution event occurs, and hence the more susceptible thin-shelled specimens in *G. sacculifer* are dissolved. Because this vulnerable portion of the species assemblage carries a "light" $\delta^{18}O$ signal, the result of selective destruction is an approach of the average *G. sacculifer* values toward the average values of *Pulleniatina.*

This tentative explanation of the difference pattern, however, does not agree with the sedimentation rate pattern. The ISR (top curve in Fig. 19) is at a minimum during deglaciation (when preservation is thought to be best), and is high during reglaciation (when dissolution is relatively strong). Thus, other factors enter also, presumably variations in productivity and thermocline motions. We cannot, without detailed analysis, offer ready explanations for the patterns seen.

Proceeding with the pattern inventory, we note that the five-cycle autostack for 500–1000 ka (Fig. 19B) is far less regular than the one in Figure 19A. The reason is the phase problem that arises between obliquity and eccentricity, as discussed above. The main peak now appears at 60–80 ka rather than at 20–30 ka (where a remnant peak is present, however). No clear pattern emerges in the difference (DIF) or ISR curves. The lowermost autostack (Fig. 19C) shows little evidence for the presence of an eccentricity cycle. However, the ISR record, interestingly, does seem to contain such a cycle. Thus, some part of the system (one that is involved in determining accumulation rates) presumably was responding to eccentricity in the Earth's orbit, but this did not influence the $\delta^{18}O$ record. The diatom record (Lange and Berger, this volume) supports this interpretation.

Obliquity Domain

The autostack procedure is next applied to the 41-k.y. cycle; that is, we form the average for six intervals of 41-k.y. length each, setting the beginning of each interval equal to zero. Six such stacks are present (Figs. 20A–20F). Four out of the six (Figs. 20A and 20D–20F) show good cycles; two (Figs. 20B and 20C) do not. The poor showings are for the interval between 250 and 750 ka, which includes intervals where the obliquity cycles are poorly expressed (Fig. 17).

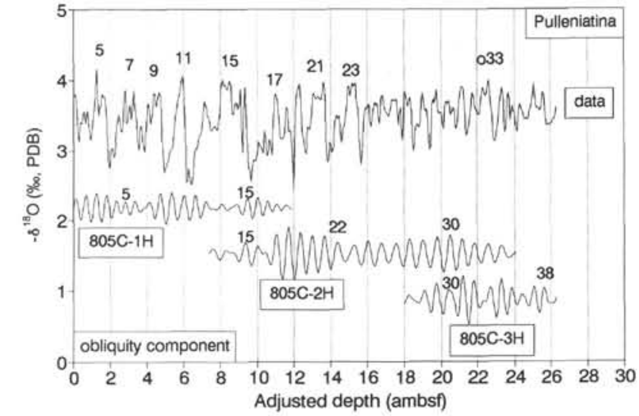

Figure 14. Summary of obliquity cycle counting in the $\delta^{18}O$ record of *Pulleniatina* in Hole 805C, down to obliquity cycle 38. Compare with Figure 10.

The peak for the first six cycles appears at 10–15 ka (Fig. 20A); the difference in $\delta^{18}O$ values is great during deglaciation (as in the eccentricity stack) and at a minimum during glacial conditions (rather than during reglaciation as in the eccentricity stack). The ISR is flat, as it should be, as its variations are not resolved for the obliquity cycle. It is between 1.3 and 1.4 cm/k.y. for the last 250 ka.

The cycles between 250 and 500 ka do not stack well (Fig. 20B). The trough for these cycles apparently is near 20 ka. The DIF is at a maximum during deglaciation (20–10 ka), but it is high earlier, too. The reglaciation minimum appears at roughly the expected position (40–30 ka). The ISR is near 1.6 cm/k.y. The next six cycles (Fig. 20C) are not well expressed. The DIF is at maximum during reglaciation and has no distinct minimum. Thus, it does not follow the expected pattern of high DIF during deglaciation and low DIF during reglaciation. The ISR is near 1.8 cm/k.y.

The next deeper six cycles (750–1000 ka; Fig. 20C) stack nicely. The interglacial peak appears near 35 ka. Thus, the DIF maximum between 5 and 10 ka corresponds to deglaciation (i.e., it occurs at 11–16 ka before the peak). POX clearly lags SOX by about 5 k.y. The minimum DIF is at 32 ka, just after the peak, but it is not very well expressed: the only strong excursion from the background is the maximum, lasting about 15% of the cycle. The next six cycles (1000–1250 ka; Fig. 20E) again stack very well. The DIF does not change much, and the ISR remains near 1.8 cm/k.y. The same pattern emerges for the next deeper six cycles (Fig. 20F), except that ISR falls back to 1.6 cm/k.y.

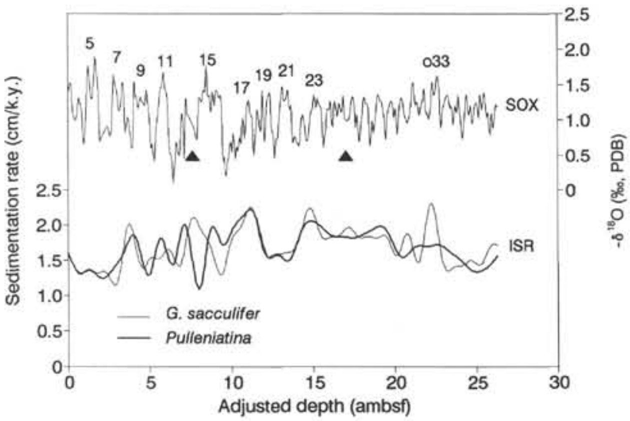

Figure 15. Instantaneous sedimentation rates (ISR) resulting from counting obliquity-related cycles in the $\delta^{18}O$ records of *G. sacculifer* and *Pulleniatina*. The curves shown represent low-order Fourier fits to the raw ISRs taken from the data in Figures 10 and 14. *G. sacculifer* $\delta^{18}O$ record shown for orientation (scale on right). Isotope stages as in Figure 3; "o33" = crest of 33rd obliquity cycle (most recent crest is set at zero). Core breaks shown by triangles.

COMPARISON OF OXYGEN ISOTOPE RECORDS HOLES 805C VS. 806B

Overview

The significance of differences in the $\delta^{18}O$ records of *G. sacculifer* and *Pulleniatina* in Hole 805C can only emerge when they are compared with the corresponding records in Hole 806B, which is at a shallower depth and in which sediments have experienced much less dissolution. A direct comparison of the oxygen isotope records, noting the differences in the values for the dissolution-sensitive species *G. sacculifer* should yield useful information on the stratigraphy of dissolution. To this end, of course, correlation between the two sites must be on a reasonably fine time scale; otherwise, only the most general results will emerge.

Correlation of the two Quaternary signals is quite straightforward in the upper part, where the mixture of eccentricity- and obliquity-related fluctuations yields unique stratigraphic patterns (Fig. 21). However, in the lower half of the Quaternary, where obliquity dominates entirely, the very uniformity and lack of differentiating character reduces the chances for correct correlation between peaks, unless complete and undisturbed sequences can be assumed. (It might be surmised that detailed biostratigraphic correlation will eventually provide the exact match between cycles. This presupposes that differential dissolution in Site 805 does not affect the datum levels used.) In Figure 21, one can see that the match back to Stage 17 poses no problems; a small gap must be assumed between Cores 130-806B-1H and -2H within Stage 9 (as shown). Dividing the depths of Core 130-806B-1H by 1.45, and those of Core 130-806B-2H by 1.37 then provides the match seen. It becomes evident that Stage 19 is missing in Hole 806B, so one has to assume that quite a substantial gap exists between Cores 130-806B-2H and -3H. To match the record below this gap to that of Hole 805C, the depths in Core 130-806B-3H are divided by 1.30. One obliquity cycle seems to be missing between Cores 130-806B-3H and -4H. After adjustment, the depths for Core 130-806B-4H are divided by 1.40 to get the match shown.

Using the gap estimates for Hole 806B that are derived in the fashion illustrated, by matching the *G. sacculifer* $\delta^{18}O$ records, we can now construct a detailed age model for the Quaternary $\delta^{18}O$ record in Hole 806B by counting obliquity-related cycles, as illustrated above for Hole 805C. After this is done (see Berger et al., this volume), the two *G. sacculifer* records can be compared in some detail (Fig. 22A). The difference (calculated for periods >86 k.y. only) is shown to be substantial in places (typically as much as 0.3‰–0.4‰). Also, the difference record is seen to contain cycles of a period close to eccentricity. An unknown (and potentially important) portion of the power in these cycles may be the result of small mismatches in the correlation, however. Wherever a slight mismatch in phase occurs, one transition (e.g., deglaciation) will show a diminished difference between the records, whereas the opposite one (e.g., reglaciation) will show an increased one. Mismatch of peaks (e.g., in Stage 15) also can reverse the sign of the difference. No physical explanation is evident for such a reversal of sign.

To illustrate this point regarding the importance of small misalignments and resulting phase shifts, we compare the two *G. sacculifer* records in the eccentricity domain (Fig. 22B). The window used for synthesis is as before (87–118 k.y.). The overall similarity of the two records in this band is quite striking. The Site 805 record is distinctly offset from the Site 806 record throughout, as might be expected from differential dissolution. The phase shifts between the two records provide the fluctuations seen: the mean of the difference is steady (by definition, as any long-term variations are filtered out). Note the change in phase near 300 ka. It may be doubted that the correlation between the two records is so exact that the sense of the phase shifts can be taken at face value. If, however, there is some reality to the phase shifts, then changes in this shift would reflect profound changes in the workings of the system: there is a great difference between having dissolution increased during deglaciation and increasing it during reglaciation.

To what extent are the differences in $\delta^{18}O$ between the two records (Fig. 22A) reflected in the $\delta^{18}O$ record of Hole 805C alone? One would expect some kind of correspondence between the SOX-SOX difference between sites and the POX-SOX difference in the deeper site, which has experienced the dissolution providing for the separation of *G. sacculifer* values in the first place. This possibility is considered in Figure 23, where the difference in SOX between sites is compared with the difference (SOX-POX) within the deeper site. The two curves correlate quite nicely in the early Quaternary, at least in the general trends, with periods greater than eccentricity. Whenever the difference between sites increases (because of dissolution effects), the difference between SOX and POX in Hole 805C has a tendency to approach zero (as expected). However, in the late Quaternary, the SOX-POX difference becomes more pronounced, despite a rather high level of site-to-site difference. Thus, a primary increase in the difference between the two taxa (a rise of the thermocline) must be assumed here.

The SOX difference signal suggests the existence of an interval of strong carbonate dissolution in the lower half of the Brunhes Chron. The intervals are marked MBDI (for mid-Brunhes dissolution interval) and EBDI (for early Brunhes dissolution interval). Also, there is an indication of a dissolution interval in the early Matuyama (labeled EMDI).

If these dissolution intervals are real, the sedimentation rate within Hole 805C should be reduced here beyond the general reduction, which is tied to the greater depth of this site. The stratigraphy of sedimentation rate ratios (Fig. 24) does not show the expected response (a strong positive excursion during the dissolution intervals), except for the early Matuyama Event. In fact, although correlations in the expected sense exist over much of the Quaternary, there is a hint of anticorrelation in the middle and lower Brunhes. That is, differences in sedimentation rates between the two sites decrease at the very time when the effects of differential dissolution increase. This seems totally incompatible with a straightforward effect of carbonate dissolution on sedimentation rate. One explanation would be that during a dissolution pulse the shallower site is proportionally more affected than the deeper one, for example, by increased winnowing or from productivity-related effects.

SUMMARY AND CONCLUSIONS

The western equatorial Pacific is of special interest in the context of Quaternary climate because it is a region of maximum open-ocean

Table 3. Age model for Quaternary oxygen isotope record of Hole 805C, *G. sacculifer* and *Pulleniatina*.

Age (ka)	*G. sacculifer* neg ^{18}O	*Pulleniatina* neg ^{18}O	Age (ka)	*G. sacculifer* neg ^{18}O	*Pulleniatina* neg ^{18}O	Age (ka)	*G. sacculifer* neg ^{18}O	*Pulleniatina* neg ^{18}O	Age (ka)	*G. sacculifer* neg ^{18}O	*Pulleniatina* neg ^{18}O
4	1.46	1.10	312	1.33	1.08	620	0.97	0.65	928	1.15	1.15
8	1.51	1.07	316	1.28	0.94	624	0.51	0.14	932	1.30	1.15
12	1.51	0.90	320	1.27	0.99	628	0.47	0.05	936	1.29	1.15
16	1.33	0.62	324	1.26	1.10	632	0.39	–0.03	940	1.21	1.24
20	1.10	0.42	328	1.21	1.13	636	0.21	–0.13	944	1.31	1.22
24	1.04	0.57	332	1.27	1.08	640	0.35	0.07	948	1.23	1.24
28	1.01	0.70	336	1.40	0.88	644	0.44	0.17	952	1.19	0.99
32	1.00	0.70	340	1.42	0.49	648	0.54	0.15	956	1.16	0.89
36	1.05	0.76	344	1.30	0.08	652	0.69	0.20	960	0.86	0.44
40	1.15	0.84	348	1.16	–0.01	656	0.57	0.37	964	0.60	0.09
44	1.26	0.78	352	0.93	0.05	660	0.75	0.40	968	0.80	0.36
48	1.32	0.70	356	0.68	0.08	664	0.69	0.35	972	0.97	0.67
52	1.29	0.78	360	0.62	0.15	668	0.45	0.30	976	1.14	0.87
56	1.21	0.86	364	0.66	0.23	672	0.61	0.34	980	1.15	0.90
60	1.14	0.75	368	0.49	0.30	676	0.59	0.55	984	1.20	0.92
64	0.96	0.57	372	0.45	0.32	680	0.74	0.27	988	1.24	0.93
68	0.73	0.46	376	0.69	0.34	684	0.68	0.27	992	0.93	0.69
72	0.65	0.50	380	0.92	0.49	688	0.92	0.44	996	1.10	0.72
76	0.84	0.69	384	1.08	0.69	692	0.90	0.31	1000	1.27	0.88
80	1.07	0.80	388	1.21	0.81	696	0.78	0.39	1004	1.21	0.98
84	1.34	0.92	392	1.35	0.95	700	1.03	0.92	1008	1.06	0.95
88	1.62	1.26	396	1.45	1.05	704	1.27	1.11	1012	1.20	0.96
92	1.74	1.40	400	1.53	1.13	708	1.24	1.01	1016	1.23	0.77
96	1.61	1.11	404	1.66	1.27	712	1.09	0.80	1020	1.14	0.79
100	1.41	0.83	408	1.61	1.35	716	0.93	0.51	1024	1.16	1.06
104	1.32	0.83	412	1.44	1.22	720	0.52	0.47	1028	1.34	1.06
108	1.31	0.94	416	1.38	0.84	724	0.65	0.48	1032	1.13	0.92
112	1.40	1.07	420	1.19	0.24	728	1.05	0.62	1036	1.01	0.85
116	1.63	1.08	424	0.88	–0.15	732	1.12	0.91	1040	0.99	0.82
120	1.87	1.06	428	0.62	–0.04	736	0.99	0.76	1044	0.99	0.79
124	1.85	1.07	432	0.52	–0.01	740	0.85	0.57	1048	1.03	0.83
128	1.73	0.98	436	0.47	–0.12	744	1.03	0.58	1052	1.17	0.97
132	1.65	0.75	440	0.21	–0.19	748	1.39	0.44	1056	1.30	1.03
136	1.38	0.43	444	0.15	–0.11	752	1.01	–0.11	1060	1.34	1.02
140	0.97	0.15	448	0.37	0.08	756	0.73	0.07	1064	1.22	1.02
144	0.71	0.06	452	0.59	0.26	760	0.92	0.87	1068	0.94	0.99
148	0.69	0.19	456	0.69	0.34	764	1.17	1.10	1072	1.00	0.76
152	0.74	0.31	460	0.61	0.32	768	1.31	1.16	1076	0.95	0.76
156	0.80	0.33	464	0.51	0.39	772	1.35	1.24	1080	0.69	0.89
160	0.82	0.27	468	0.58	0.49	776	1.40	1.18	1084	0.78	0.54
164	0.82	0.21	472	0.89	0.51	780	1.25	0.92	1088	0.97	0.75
168	0.85	0.31	476	1.09	0.57	784	0.93	0.55	1092	1.19	1.13
172	0.89	0.50	480	0.83	0.75	788	0.83	0.46	1096	1.34	1.04
176	0.90	0.66	484	0.59	0.98	792	0.65	0.34	1100	1.27	0.95
180	0.91	0.77	488	1.26	0.96	796	0.46	0.25	1104	1.23	1.00
184	0.89	0.79	492	1.22	0.85	800	0.61	0.50	1108	1.23	1.04
188	0.84	0.73	496	1.06	0.77	804	0.73	0.63	1112	1.09	0.82
192	0.78	0.62	500	1.04	0.70	808	0.76	0.60	1116	0.71	0.40
196	0.82	0.57	504	0.99	0.59	812	0.92	0.69	1120	0.84	0.40
200	1.00	0.66	508	0.96	0.59	816	1.12	0.90	1124	0.93	0.60
204	1.29	0.89	512	0.92	0.63	820	1.31	1.09	1128	0.82	0.68
208	1.55	1.10	516	0.88	0.65	824	1.46	1.08	1132	0.94	0.65
212	1.60	1.02	520	0.83	0.62	828	1.43	1.05	1136	1.14	0.65
216	1.50	0.78	524	0.74	0.59	832	1.30	1.05	1140	1.31	0.89
220	1.44	0.70	528	0.76	0.66	836	1.27	1.07	1144	1.36	1.13
224	1.41	0.78	532	1.09	0.90	840	1.31	1.06	1148	1.29	0.97
228	1.29	0.91	536	1.31	1.16	844	1.39	1.03	1152	1.27	0.86
232	1.17	0.92	540	1.29	1.30	848	1.42	1.03	1156	1.23	0.88
236	1.13	0.75	544	1.26	1.26	852	1.29	1.12	1160	1.11	0.69
240	1.21	0.85	548	1.32	1.22	856	1.16	1.25	1164	0.90	0.36
244	1.39	1.12	552	1.41	1.22	860	1.22	1.23	1168	0.74	0.41
248	1.52	1.00	556	1.39	1.16	864	0.95	0.81	1172	0.99	0.84
252	1.36	0.79	560	1.60	1.19	868	0.69	0.31	1176	1.16	1.02
256	0.93	0.64	564	1.66	1.27	872	0.75	0.14	1180	1.21	1.03
260	0.86	0.36	568	1.35	1.22	876	0.75	0.27	1184	1.26	1.16
264	0.98	0.46	572	1.35	0.93	880	0.71	0.39	1188	1.26	0.99
268	1.00	0.65	576	1.19	0.80	884	0.66	0.29	1192	1.16	0.84
272	0.85	0.50	580	1.20	0.91	888	0.63	0.31	1196	1.03	0.82
276	0.79	0.30	584	1.40	0.98	892	0.71	0.53	1200	1.13	0.83
280	0.60	0.40	588	1.24	0.91	896	0.94	0.75	1204	1.05	0.73
284	0.99	0.72	592	1.29	0.92	900	1.08	0.79	1208	0.82	0.61
288	1.53	0.96	596	1.42	1.09	904	0.99	0.76	1212	0.95	0.82
292	1.42	0.90	600	1.41	1.04	908	0.88	0.74	1216	1.15	0.99
296	1.31	0.72	604	1.36	0.47	912	0.71	0.42	1220	1.26	0.96
300	1.21	0.74	608	1.32	0.56	916	0.76	0.55	1224	1.32	1.00
304	1.18	0.96	612	1.32	1.18	920	0.91	0.68	1228	1.30	0.96
308	1.28	1.11	616	1.31	1.12	924	1.07	0.83	1232	1.22	0.83

Table 3 (continued).

Age (ka)	*G. sacculifer* neg ^{18}O	*Pulleniatina* neg ^{18}O	Age (ka)	*G. sacculifer* neg ^{18}O	*Pulleniatina* neg ^{18}O
1236	1.10	0.85	1420	1.20	1.12
1240	1.02	0.91	1424	1.11	0.84
1244	0.99	0.84	1428	1.18	0.77
1248	0.96	0.68	1432	1.33	0.90
1252	1.03	0.64	1436	1.26	0.90
1256	1.16	0.81	1440	1.08	0.82
1260	1.23	1.02	1444	0.90	0.74
1264	1.43	1.16	1448	0.77	0.62
1268	1.54	1.20	1452	0.76	0.59
1272	1.36	1.18	1456	0.87	0.75
1276	1.22	1.05	1460	1.08	0.93
1280	1.25	0.73	1464	1.28	0.93
1284	1.24	0.51	1468	1.36	0.89
1288	1.13	0.56	1472	1.24	0.85
1292	1.07	0.65	1476	1.12	0.79
1296	1.14	0.73	1480	1.10	0.75
1300	1.23	0.95	1484	1.18	0.76
1304	1.34	1.12	1488	1.14	0.76
1308	1.45	1.03	1492	0.99	0.74
1312	1.26	0.92	1496	1.01	0.79
1316	1.08	0.86	1500	1.15	0.87
1320	1.07	0.84	1504	1.21	0.93
1324	1.01	0.81	1508	1.24	1.04
1328	1.16	0.96	1512	1.23	1.20
1332	1.44	1.13	1516	1.15	1.19
1336	1.49	1.18	1520	1.05	1.02
1340	1.36	1.10	1524	1.14	0.91
1344	1.48	1.12	1528	1.33	0.91
1348	1.61	1.27	1532	1.27	0.90
1352	1.61	1.20	1536	1.16	0.89
1356	1.34	0.98	1540	1.26	0.87
1360	0.97	0.81	1544	1.36	0.94
1364	0.90	0.59	1548	1.35	1.08
1368	1.08	0.44	1552	1.19	1.11
1372	1.19	0.43	1556	1.04	0.99
1376	1.26	0.53	1560	1.10	0.78
1380	1.30	0.68	1564	1.02	0.66
1384	1.34	0.84	1568	0.83	0.66
1388	1.35	0.99	1572	0.99	0.68
1392	1.32	1.14	1576	1.08	0.68
1396	1.24	1.17	1580	0.91	0.68
1400	1.16	1.01	1584	1.01	0.73
1404	1.20	0.70	1588	1.17	0.76
1408	1.09	0.58	1592	1.22	0.78
1412	0.95	0.76	1596	1.20	0.88
1416	1.07	1.03	1600	1.16	0.90

Notes: Derived from Table 1 by adjusting for expansion in core and coring gaps and from age assignments based on counting obliquity-related cycles.

temperatures with very little seasonal variation. The mechanisms responsible for keeping surface-water temperatures at rather uniform high temperatures throughout the year may likewise be expected to minimize variation through glacial-interglacial cycles, so that most of the stable isotope record in the area should reflect phenomena of global significance rather than regional temperature variations. On the other hand, fluctuations in thermocline depth and upwelling are expected for this area, which is part of the equatorial upwelling system in the Pacific, which in itself constitutes a major element in global climate dynamics. The oxygen isotope record at Site 805, then, is dominated by a global signal of Quaternary ice-volume variation, modified by surface-water temperature fluctuations and by changes in regional thermocline depth. Also, this site is deep enough (3188 m) to be affected by carbonate dissolution, which in turn influences the oxygen isotope record.

We estimate the relative importance of the four signals (global ice volume, regional temperature, regional thermocline, deep-water saturation) in the present data as follows, in terms of proportion of range of $\delta^{18}O$ values controlled within the late Quaternary:

Global ice volume	1.1‰	73%
Temperature change	0.2‰	13%
Thermocline change	0.1‰	7%
Dissolution change	0.1‰	7%
Total	1.5‰	100%

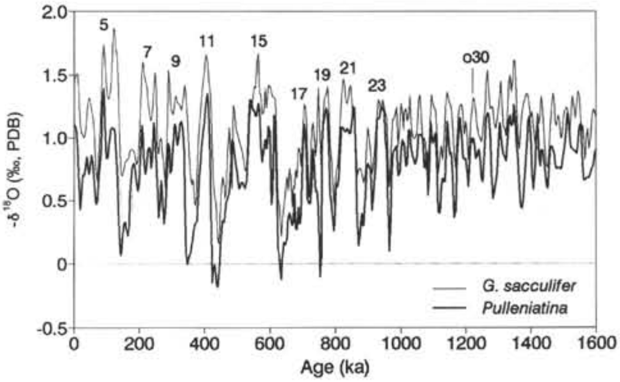

Figure 16. Age model for the $\delta^{18}O$ records of *G. sacculifer* and *Pulleniatina* in Hole 805C, Cores 130-805C-1H through -3H. Isotope stages as in Figure 3; "o30" = crest of 30th obliquity cycle (most recent crest is o0).

The ice-volume effect may be slightly greater, with other factors compensating through opposite sign. Stratigraphic separation of these various effects is only possible if enough proxy variables are available. It cannot be done with only the three variables considered here ($\delta^{18}O$ of *G. sacculifer*, $\delta^{18}O$ of *Pulleniatina*, and instantaneous sedimentation rate). Fluctuations in productivity and dissolution must be explored using additional proxies. Time constraints prevented us from doing this in the present study.

The difficulties arising are illustrated by the fact that differences in $\delta^{18}O$ values between *G. sacculifer* and *Pulleniatina* are a result of changes in mixed layer thickness as well as differential dissolution, with *Pulleniatina* having the deeper habitat and also being more resistant to dissolution than *G. sacculifer*.

Comparisons with Hole 806B are especially useful when studying dissolution effects on the oxygen isotope record because of the shallow position of this site (2520 m). The effect is reflected in a difference in $\delta^{18}O$ values for *G. sacculifer*, due to the fact that ^{18}O-rich shells become concentrated in Site 805 through differential removal of isotopically light specimens. Surprisingly, the variations of this difference between the two sites is not closely correlated with sedimentation rate ratios. Thus, factors other than dissolution of carbonate dominate accumulation rates in Site 805.

The main stratigraphic trends that emerge are as follows:

1. The last third of the Quaternary is characterized by strong, regular, climatic fluctuations dominated by 100- and 41-k.y. periods.
2. The early part of the Quaternary oxygen isotope record has essentially no information in the 100-k.y. band, but it is entirely dominated by obliquity-related fluctuations.
3. The middle of the period is transitional.

There is a confusing zone between Stages 17 and 21, with an odd phase reversal in the eccentricity-related signal (E7 to E8), that produces a mismatch in the progression of counts based on eccentricity and obliquity. It is not clear whether this irregularity is a result of problems in recovery, in the record itself, or in the analysis attempted here. The problem prevents us from assigning a unique age to the Brunhes/Matuyama boundary, which is either near 790 ka or near 830 ka, by our counts. We have used the more conservative lower age for our age model (794 ka, to be exact), in agreement with Shackleton et al. (1990).

Isotopic Stages 11–13 and 16–17 are characterized by large differences in $\delta^{18}O$ of *G. sacculifer* at Sites 805 and 806, indicating strong dissolution. Also, differences are large below o33, near 1500 ka.

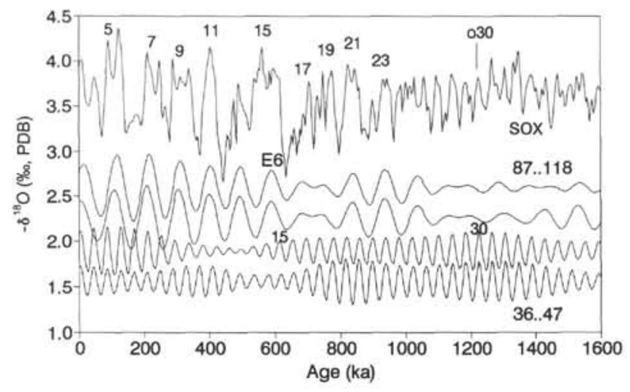

Figure 17. Fourier analysis of $\delta^{18}O$ records of *G. sacculifer* and *Pulleniatina* in the time domain, showing eccentricity-related (87–118 k.y.) and obliquity-related (36–47 k.y.) fluctuations. In each pair, the upper curve is from *G. sacculifer*, the lower from *Pulleniatina*. The record of *G. sacculifer* in Hole 805C is given for orientation (arbitrary scale). "E6" = crest of sixth eccentricity cycle (most recent crest is set at zero). Crests of 15th and 30th obliquity cycles are marked.

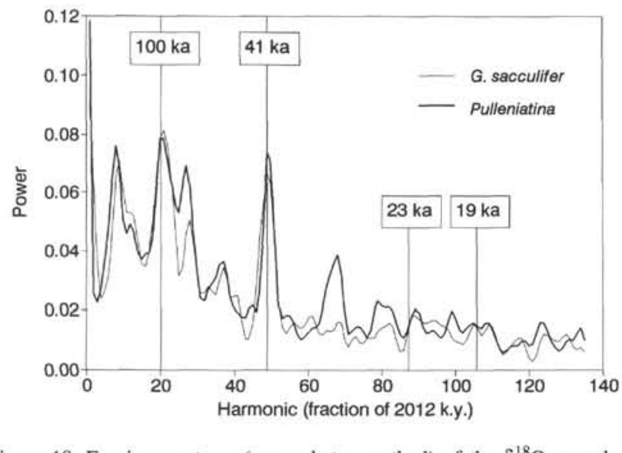

Figure 18. Fourier spectrum (somewhat smoothed) of the $\delta^{18}O$ records of *G. sacculifer* and *Pulleniatina*, based on analysis of the age models of these records, extended to 2012 k.y. (by adding mean values on both ends). The positions of the orbital periods (100, 41, 23, and 19 k.y.) are shown for orientation. The orbital period (41 k.y.) is the basis for the age model, so that a strong peak at 41 k.y. is expected from the dating method.

ACKNOWLEDGMENTS

We thank the members of the shipboard party of Leg 130 for assistance in sampling and other help rendered during the cruise. Dr. M. Segl, Bremen, supervised and facilitated the generation of the isotope data. Tom Janecek provided the GRAPE data used for checking on core breaks. We are indebted to Eystein Jansen and Richard Corfield for reading the draft manuscript and making helpful suggestions. Financial support was provided by the U.S. National Science Foundation and by the Deutsche Forschungsgemeinschaft.

Note added in proof: The nannofossil data of Takayama (this volume) suggest a 2-m coring gap between Cores 130-805C-2H and -3H. If real, such a gap would affect some of the conclusions regarding that part of the record that is older than 1 m.y.

REFERENCES*

Baksi, A., Houghton, B., McWilliams, M., Tanaka, H., and Turner, G., 1991. What is the age of the Brunhes-Matuyama polarity transition? *Geol. Soc. Am. Abstr. Progr.*, GP32B:135.

Baksi, A.K., Hsu, V., McWilliams, M.O., and Farrar, E., 1992. $^{40}Ar/^{39}Ar$ dating of the Brunhes-Matuyama geomagnetic field reversal. *Science,* 256:356–357.

Berger, A.L., 1984. Accuracy and frequency stability of the Earth's orbital elements during the Quaternary. *In* Berger, A., Imbrie, J., Hays, J., Kukla, G., and Saltzman, B. (Eds.), *Milankovitch and Climate* (Pt. 1): *Understanding the Response to Astronomical Forcing:* Dordrecht (D. Reidel), 3–39.

Berger, W.H., Bonneau, M.C., and Parker, F.L., 1982. Foraminifera on the deep-sea floor: lysocline and dissolution rate. *Oceanol. Acta,* 5:249–258.

Berger, W.H., and Gardner, J.V., 1975. On the determination of Pleistocene temperatures from planktonic foraminifera. *J. Foraminiferal Res.,* 5:102–113.

Berger, W.H., Killingley, J.S., and Vincent, E., 1978. Stable isotopes in deep-sea carbonates: Box Core ERDC92, west equatorial Pacific. *Oceanol. Acta,* 1:203–216.

————, 1987. Time scale of Wisconsin/Holocene transition: oxygen isotope record in the western equatorial Pacific. *Quat. Res.,* 28:295–306.

Berger, W.H., Kroenke, L.W., Mayer, L.A., and Shipboard Scientific Party, 1991. Ontong Java Plateau, Leg 130: synopsis of major drilling results. *In* Kroenke, L.W., Berger, W.H., Janecek, T.R., et al., *Proc. ODP, Init. Repts.,* 130: College Station, TX (Ocean Drilling Program), 497–537.

Berger, W.H., and Mayer, L.A., 1987. Cenozoic paleoceanography 1986: an introduction. *Paleoceanography,* 2:613–623.

Berger, W.H., and Wefer, G., 1992. Klimageschichte aus Tiefseesedimenten—Neues vom Ontong Java Plateau (Westpazifik). *Naturwissenschaften.,* No. 79.

CLIMAP Project Members, 1976. The surface of the ice-age earth. *Science,* 191:1131–1137.

Emiliani, C., 1955. Pleistocene temperatures. *J. Geol.,* 63:538–578.

Epstein, S., Buchsbaum, R., Lowenstam, H.A., and Urey, H.C., 1953. Revised carbonate-water isotopic temperature scale. *Geol. Soc. Am. Bull.,* 64:1315–1325.

Epstein, S., and Mayeda, T., 1953. Variation of O^{18} content of waters from natural sources. *Geochim. Cosmochim. Acta,* 4:213–224.

Groetsch, J., Wu, G., and Berger, W.H., 1991. Carbonate cycles in the Pacific: reconstruction of saturation fluctuations. *In* Einsele, G., Ricken, W., Seilacher, A. (Eds.), *Cycles and Events in Stratigraphy:* Berlin (Springer-Verlag), 110–125.

Hays, J.D., Imbrie, J., and Shackleton, N.J., 1976. Variations in the Earth's orbit: pacemaker of the ice ages. *Science,* 194:1121–1132.

Hebbeln, D., Wefer, G., and Berger, W.H., 1990. Pleistocene dissolution fluctuations from apparent depth of deposition in Core ERDC-127P, west-equatorial Pacific. *Mar. Geol.,* 92:165–176.

Imbrie, J., Hays, J.D., Martinson, D.G., McIntyre, A., Mix, A.C., Morley, J.J., Pisias, N.G., Prell, W.L., and Shackleton, N.J., 1984. The orbital theory of Pleistocene climate: support from a revised chronology of the marine $\delta^{18}O$ record. *In* Berger, A., Imbrie, J., Hays, J., Kukla, G., and Saltzman, B. (Eds.), *Milankovitch and Climate* (Pt. 1): *Understanding the Response to Astronomical Forcing*: Dordrecht (D. Reidel), 269–305.

Izett, G., and Obradovich, J., 1991. Dating of the Matuyama-Brunhes boundary based on $^{40}Ar/^{39}Ar$ ages of the Bishop Tuff and Cerro San Luis rhyolite. *Geol. Soc. Am. Abstr. Progr.,* 23:A106.

Johnson, R.G., 1982. Brunhes-Matuyama magnetic reversal dated at 790,000 yr B.P. by marine-astronomical correlations. *Quat. Res.,* 17:135–147.

Johnson, T.C., Hamilton, E.L., and Berger, W.H., 1977. Physical properties of calcareous ooze: control by dissolution at depth. *Mar. Geol.,* 24:259–277.

Kroenke, L.W., Berger, W.H., Janecek, T.R., et al., *Proc. ODP, Init. Repts.,* 130: College Station, TX (Ocean Drilling Program).

Le, J., and Shackleton, N.J., 1992. Carbonate dissolution fluctuations in the western equatorial Pacific during the late Quaternary. *Paleoceanography,* 7:21–42.

Pisias, N.G., 1976. Late Quaternary sediment of the Panama Basin: sedimentation rates, periodicities, and controls of carbonate and opal accumulation. *In* Cline, R.M., and Hays, J.D. (Eds.), *Investigation of Late Quaternary Paleoceanography and Paleoclimatology.* Mem.—Geol. Soc. Am., 145:375–391.

Pisias, N.G., and Moore, T.C., 1981. The evolution of Pleistocene climate: a time series approach. *Earth Planet. Sci. Lett.,* 52:450–458.

Prell, W.L., Imbrie, J., Martinson, D.G., Morley, J.J., Pisias, N.G., Shackleton, N.J., and Streeter, H.F., 1986. Graphic correlation of oxygen stratigraphy application to the late Quaternary. *Paleoceanography,* 1:137–162.

* Abbreviations for names of organizations and publication titles in ODP reference lists follow the style given in *Chemical Abstracts Service Source Index* (published by American Chemical Society).

Ramanathan, V., Barkstrom, B.R., and Harrison, E.F., 1989. Climate and the Earth's radiation budget. *Physics Today,* 42:22–32.

Raymo, M.E., Ruddiman, W.F., Shackleton, N.J., and Oppo, D.W., 1990. Evolution of Atlantic-Pacific $\delta^{13}C$ gradients over the last 2.5 m.y. *Earth Planet. Sci. Lett.,* 97:353–368.

Ruddiman, W.F., McIntyre, A., and Raymo, M.E., 1986. Matuyama 41,000-year cycles: North Atlantic Ocean and Northern Hemisphere ice sheets. *Earth Planet. Sci. Lett.,* 80:117–129.

Schiffelbein, P., 1984. Stable isotope systematics in Pleistocene deep-sea sediment records [Ph.D dissert.]. Univ. of Calif. at San Diego, La Jolla.

Shackleton, N.J., and Opdyke, N.D., 1973. Oxygen isotope and paleomagnetic stratigraphy of equatorial Pacific Core V28-238: oxygen isotope temperatures and ice volumes on a 10^5 year and 10^6 year scale. *Quat. Res.,* 3:39–55.

————, 1976. Oxygen-isotope and paleomagnetic stratigraphy of Pacific Core V28-239: late Pliocene to latest Pleistocene. *In* Cline, R.M., and Hays, J.D. (Eds.), *Investigation of Late Quaternary Paleoceanography and Paleoclimatology.* Mem.—Geol. Soc. Am., 145:449–464.

————, 1977. Oxygen isotope and paleomagnetic evidence for early Northern Hemisphere glaciation. *Nature,* 270:216–219.

Shackleton, N.J., Berger, A., and Peltier, W.R., 1990. An alternative astronomical calibration of the lower Pleistocene time scale based on ODP Site 677. *Trans. R. Soc. Edinburgh, Earth Sci.,* 81:251–261.

Shipboard Scientific Party, 1991. Site 805. *In* Kroenke, L.W., Berger, W.H., Janecek, T.R., et al., *Proc. ODP, Init. Repts.,* 130: College Station, TX (Ocean Drilling Program), 223–290.

Wefer, G., and Berger, W.H., 1991. Isotope paleontology: growth and composition of extant calcareous species. *Mar. Geol.,* 100:207–248.

Whitman, J., and Berger, W.H., 1992. Pliocene-Pleistocene oxygen isotope record, Site 586, Ontong Java Plateau. *Mar. Micropaleontol.,* 18:171–198.

Woodruff, F., Savin, S.M., and Douglas, R.G., 1981. Miocene stable isotope record: a detailed deep Pacific Ocean study and its paleoclimatic implications. *Science,* 212:665–668.

Wu, G., and Berger, W.H., 1989. Planktonic foraminifera: differential dissolution and the Quaternary stable isotope record in the west equatorial Pacific. *Paleoceanography,* 4:181–198.

————, 1991. Pleistocene $\delta^{18}O$ records from Ontong-Java Plateau: effects of winnowing and dissolution. *Mar. Geol.,* 96:193–209.

Date of initial receipt: 27 January 1992
Date of acceptance: 1 September 1992
Ms 130B-032

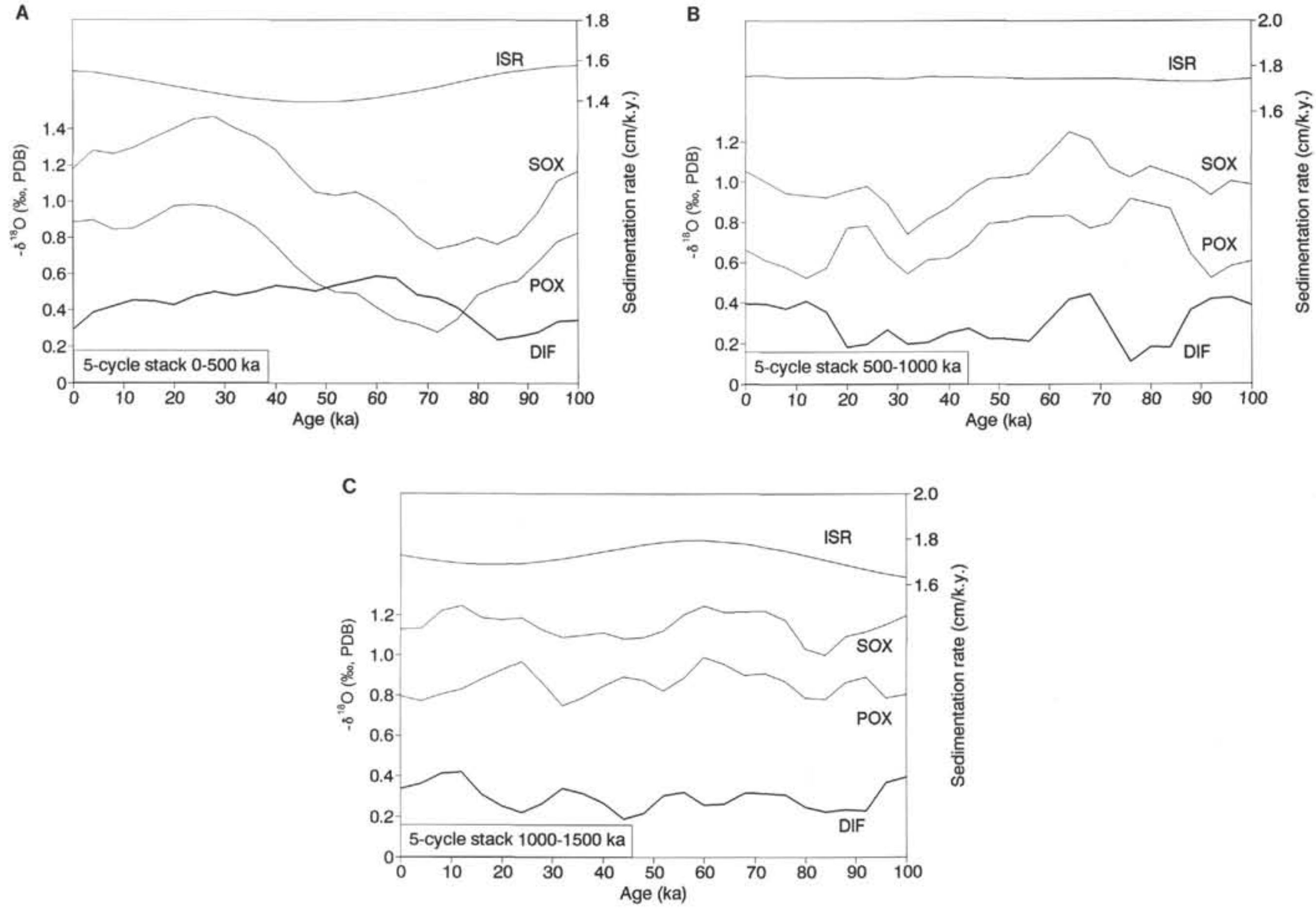

Figure 19. Stack of $\delta^{18}O$ sections of *G. sacculifer* (SOX) and *Pulleniatina* (POX) modulo 100 ka, for five intervals at a time. This "autostack" is meant to capture the essential trends in the eccentricity domain. **A.** 0–500 ka. **B.** 500–1000 ka. **C.** 1000–1500 ka. ISR = instantaneous sedimentation rate, and DIF = difference between SOX and POX.

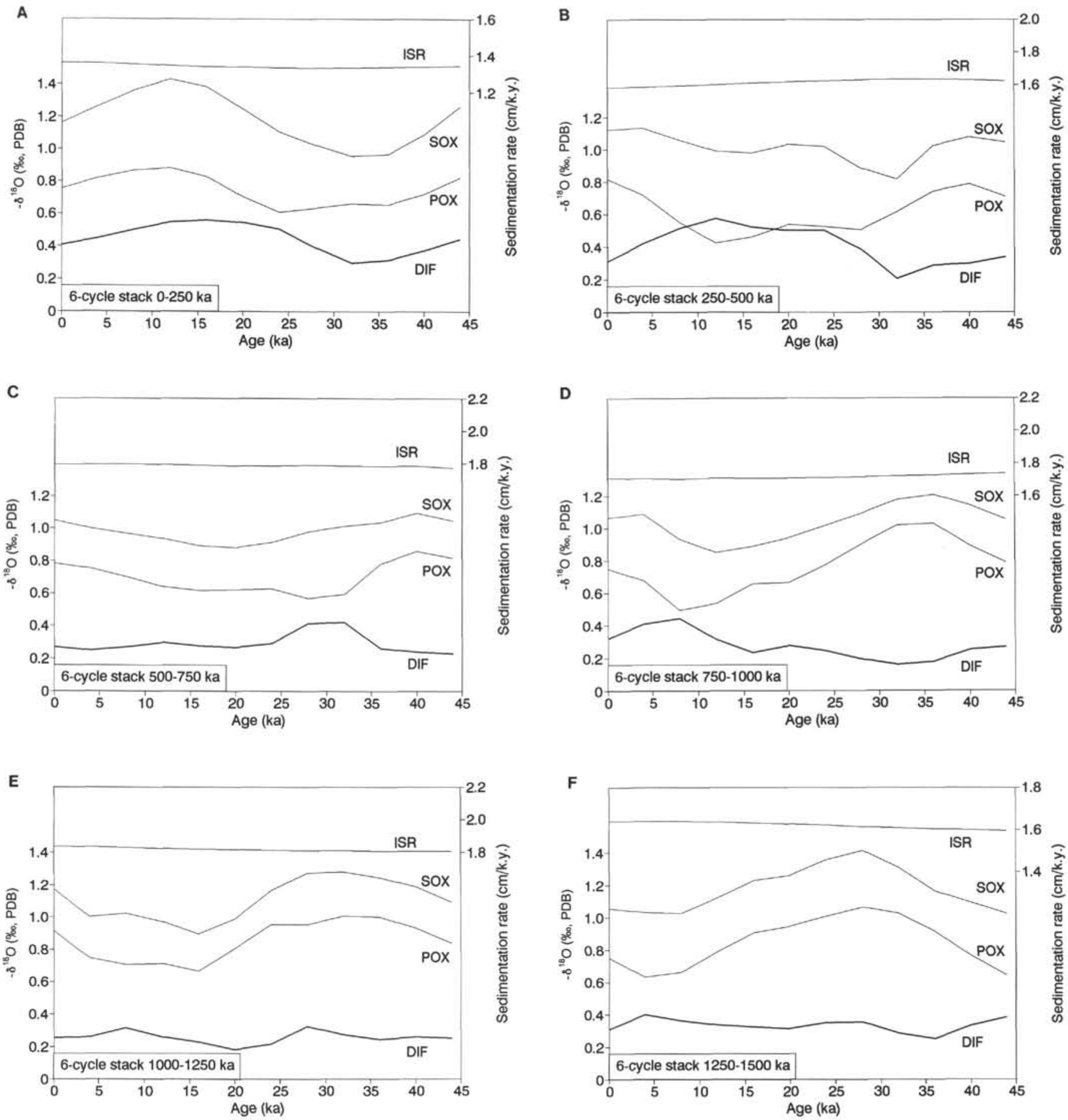

Figure 20. Stack of $\delta^{18}O$ sections of *G. sacculifer* (SOX) and *Pulleniatina* (POX) modulo 41 ka, for six consecutive intervals for the time spans shown in the lower left of the graph. **A–F.** Successively deeper sections in Hole 805C, first three cores.

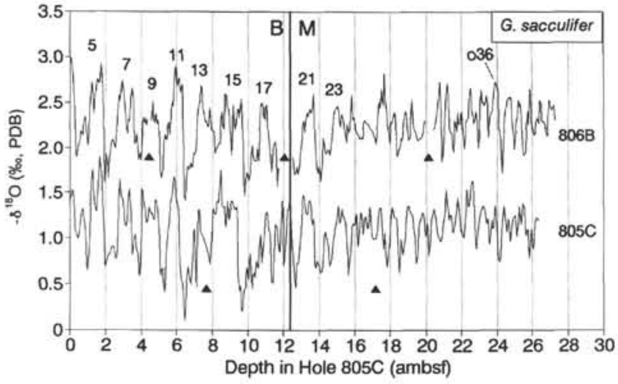

Figure 21. Correlation between the $\delta^{18}O$ records of *G. sacculifer* in Holes 806B and 805C with the depths of Site 806 adjusted to those of Site 805, using the match between the signals. Triangles indicate positions of core breaks. B = Brunhes, and M = Matuyama.

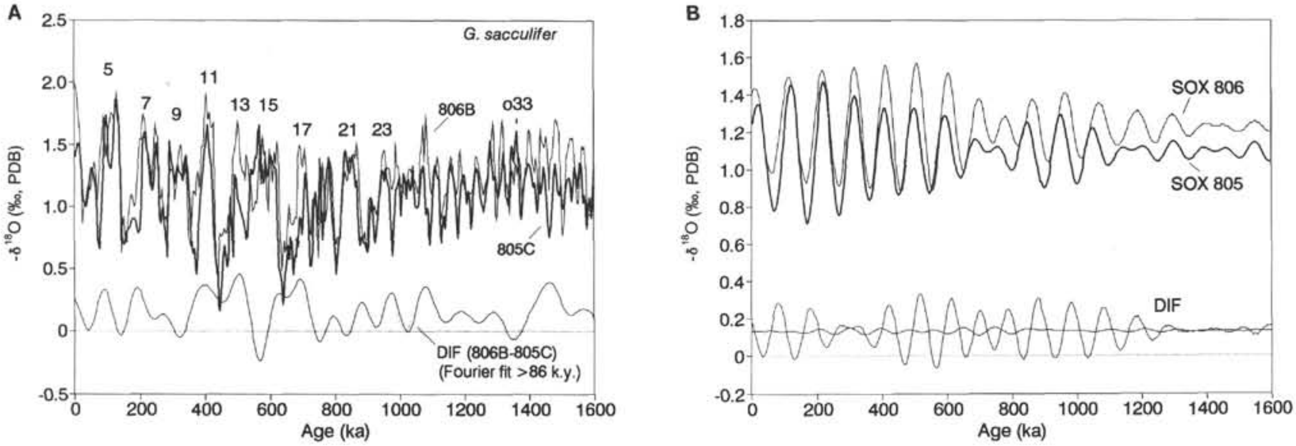

Figure 22. Comparison of the $\delta^{18}O$ records of *G. sacculifer* in Holes 805C and 806B in the time domain. **A.** Difference in $\delta^{18}O$ (DIF), with periods shorter than eccentricity eliminated. **B.** Difference in the eccentricity band, illustrating the importance of apparent phase shifts in producing apparent dissolution cycles (i.e., difference cycles). These shifts may be an artifact of analysis and correlation.

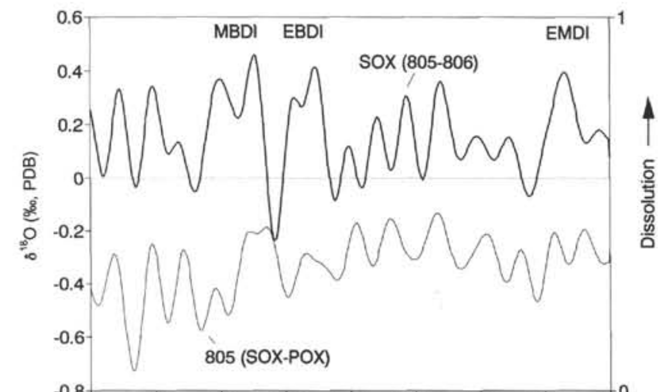

Figure 23. Comparison of difference in $\delta^{18}O$ values of *G. sacculifer* in the Quaternary records of Holes 805C and 806B (labeled SOX(805–806)) with difference in $\delta^{18}O$ values of *G. sacculifer* and *Pulleniatina* in Hole 805C (labeled 805(SOX–POX)). Dissolution effects on isotopes should produce upward excursions in either curve. MBDI = mid-Brunhes dissolution interval, EBDI = early Brunhes dissolution interval, and EMDI = early Matuyama dissolution interval.

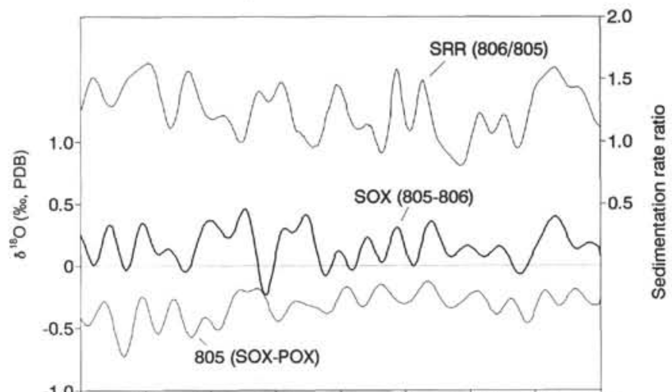

Figure 24. Comparison of presumed indices of dissolution SOX (805–806) and 805 (SOX–POX) (as in Fig. 23) with the sedimentation rate ratio between Holes 806B and 805C. A higher ratio should indicate increased removal from the deeper site (805C), relative to the shallower one (806B). Ideally, the three curves should be parallel (if dissolution effects control sedimentation rates at Site 805, relative to Site 806).